



**HAL**  
open science

## The inner dust coma of Comet 26P/Grigg-Skjellerup: multiple jets and nucleus fragments?

Neil McBride, Simon F. Green, Anny Chantal Levasseur-Regourd, Blandine Goidet-Devel, Jean-Baptiste Renard

► **To cite this version:**

Neil McBride, Simon F. Green, Anny Chantal Levasseur-Regourd, Blandine Goidet-Devel, Jean-Baptiste Renard. The inner dust coma of Comet 26P/Grigg-Skjellerup: multiple jets and nucleus fragments?. *Monthly Notices of the Royal Astronomical Society*, 1997, 289 (3), pp.535-553. 10.1093/mnras/289.3.535 . insu-02985650

**HAL Id: insu-02985650**

**<https://insu.hal.science/insu-02985650>**

Submitted on 2 Nov 2020

**HAL** is a multi-disciplinary open access archive for the deposit and dissemination of scientific research documents, whether they are published or not. The documents may come from teaching and research institutions in France or abroad, or from public or private research centers.

L'archive ouverte pluridisciplinaire **HAL**, est destinée au dépôt et à la diffusion de documents scientifiques de niveau recherche, publiés ou non, émanant des établissements d'enseignement et de recherche français ou étrangers, des laboratoires publics ou privés.

# The inner dust coma of Comet 26P/Grigg–Skjellerup: multiple jets and nucleus fragments?

Neil McBride,<sup>1</sup> Simon F. Green,<sup>1</sup> A. Chantal Levasseur-Regourd,<sup>2</sup> Blandine Goidet-Devel<sup>3</sup> and Jean-Baptiste Renard<sup>4</sup>

<sup>1</sup> *Unit for Space Sciences and Astrophysics, Physics Laboratory, University of Kent, Canterbury CT2 7NR*

<sup>2</sup> *Université Paris 6, Service d'Aéronomie CNRS, BP 3, 91371 Verrières, France*

<sup>3</sup> *Observatoire de Besançon, 41 avenue de l'observatoire, BP 1615, 25010 Besançon Cedex, France*

<sup>4</sup> *LPCE-CNRS, 3A avenue recherche scientifique, 45701 Orléans Cedex 2, France*

Accepted 1997 March 5. Received 1997 March 5; in original form 1996 July 8

## ABSTRACT

On 1992 July 10 the European Space Agency's spaceprobe *Giotto* passed the nucleus of the comparatively inactive comet 26P/Grigg–Skjellerup at a relative velocity of  $14 \text{ km s}^{-1}$ . This *Giotto* Extended Mission (GEM) followed a highly successful encounter in 1986 with Comet 1P/Halley. We present results returned from the Optical Probe Experiment (OPE) and in particular consider data gathered by the channels sensitive to the scattering of solar light by cometary dust grains, in emission-free continuum bands. Owing to the demise of the Halley Multicolour Camera (HMC) during the Halley encounter, and the low number of impacts registered by the Dust Impact Detection System (DIDSY), OPE data offer the best indication of the actual encounter geometry. We find that it is likely that *Giotto* was on the sunward side of the shadow terminator plane at closest approach, with our modelling results suggesting that *Giotto* passed  $\sim 100 \text{ km}$  from the nucleus (although distances of up to  $300 \text{ km}$  cannot be ruled out). We investigate possible causes of the striking 'spike' features, or 'events', in the OPE data. While scattering of sunlight from ejecta particles as a result of dust impacts on the spacecraft body cannot be ruled out, considerations of the hypervelocity impact mechanisms and impact geometry show that this explanation is not without problems, and more investigation is needed before it can be conclusively accepted. As an alternative solution, we find that the complex data profiles can be fitted by jet activity in the innermost coma (which was not resolvable by ground-based observers). One particular event occurring at least  $1000 \text{ km}$  from the nucleus can be fitted if the OPE line of sight passes close to a nucleus fragment of radius  $10\text{--}100 \text{ m}$  which is situated around  $50 \text{ km}$  from the spacecraft and which is producing a small dust coma.

**Key words:** instrumentation: detectors – instrumentation: miscellaneous – space vehicles – comets: general – comets: individual: 26P/Grigg–Skjellerup.

## 1 INTRODUCTION

On 1986 March 13 the European Space Agency's spaceprobe *Giotto* passed within about  $600 \text{ km}$  of the nucleus of the highly active comet 1P/Halley at a relative velocity of  $68 \text{ km s}^{-1}$ . This hazardous encounter did not leave the probe unscathed, although the condition of the spacecraft and on-board experiments was such that a second flyby of a cometary nucleus could be undertaken. On 1992 July 10 *Giotto* passed through the innermost coma of the comet 26P/Grigg–Skjellerup. This comet had an observed gas production rate that was 2 orders of magnitude less than Halley, which, partnered with the lower encounter velocity of  $14 \text{ km s}^{-1}$  (and different encounter geometry), meant that the *Giotto* Extended

Mission (GEM) promised a very different encounter from that of Comet Halley.

The spacecraft was targeted directly at the nucleus, but, owing to the uncertainties in the position of the nucleus, the actual flyby distance and geometry of the nucleus were unknown prior to encounter. The demise of the Halley Multicolour Camera (HMC) during the 1986 encounter meant the Optical Probe Experiment (OPE) was the only optical sensor active for the Grigg–Skjellerup encounter, and, without direct imaging of the nucleus, OPE would offer the best estimate of the closest approach distance of the nucleus. Although the geometry of the encounter did not permit a local inversion of the data, subsequent analysis has indicated that the dust coma was entered at a distance of at least  $20\,000 \text{ km}$  from

the nucleus (Levasseur-Regourd et al. 1993a). The reduced relative velocity (compared with the Halley encounter) has allowed an excellent spatial resolution (14 km parallel to the trajectory) to be obtained as the line of sight of the OPE telescope passes through the inner coma. This has enabled the detection of some unexpected and striking inner coma features.

In this paper, we present the results obtained by OPE at the Grigg–Skjellerup encounter from the dust continuum channels, with particular reference to possible explanations for the unusual features in the data.

## 2 GRIGG–SKJELLERUP FLYBY GEOMETRY

The OPE had been proposed and selected for the *Giotto* spacecraft mission to Comet 1P/Halley to provide the first *in situ* measurements of brightness and polarization from within a cometary coma (Levasseur-Regourd et al. 1984). The operation of the experiment relied on the fact that if the line of sight of the optical telescope was parallel to the spacecraft trajectory and if the coma is optically thin then the difference between two consecutive measurements is directly proportional to the light scattered by dust or emitted by gases inside a small volume element centred on the moving probe (Levasseur-Regourd et al. 1981). The geometry of the Halley encounter meant that the phase angle of the OPE observations (the Sun–scattering particle–OPE angle) would be equal to either  $107.2^\circ$  (for forward viewing with respect to the probe’s motion) or  $72.8^\circ$  (for rearward viewing). Since typical phase curves are rather flat in the  $70^\circ$  to  $110^\circ$  domain, almost no additional information would have been obtained from measurements performed in both directions. A rearward-looking instrument was chosen, to avoid the inevitable damage that would occur as a result of dust impacts on a forward-looking instrument.

The *Giotto* encounter with Comet Grigg–Skjellerup differed from that with Halley in two major respects. Since Grigg–Skjellerup has a prograde orbit (unlike Halley), the relative velocity at encounter was about five times lower, with the comet overtaking the spacecraft, approaching from south of the ecliptic. In addition, the spacecraft’s spin axis (which was parallel to the OPE line-of-sight axis) was not aligned with the relative velocity vector as it had been at Halley, but was oriented at an angle of  $68.8^\circ$ . This was because of the requirements for pointing the communication high-gain antenna towards the Earth and the fact that the spacecraft’s cylindrical solar array had to be perpendicular to the Sun direction to maximize available power. Such a geometry produced a phase angle for dust particles observed by OPE of  $90.4^\circ$  (see Fig. 1). The observed polarization is at a maximum when the phase angle is around  $90^\circ$  (Levasseur-Regourd 1992) and so the Grigg–Skjellerup encounter offered a favourable geometry for retrieving the polarization data with maximum signal-to-noise ratio. The heliocentric and geocentric distances of the comet were 1.01 and 1.43 au respectively (compared to 0.90 and 0.96 au respectively at the Halley flyby, with a phase angle of  $72.8^\circ$ ).

In order to interpret the OPE data it is essential to understand the geometry of the Grigg–Skjellerup encounter, and this is shown in Fig. 1. An orthogonal frame is shown centred on the nucleus such that the  $x$ -axis points to the Sun. The  $y$ -axis is such that the  $x$ - $y$  plane is parallel to *Giotto*’s trajectory vector, which makes an angle of  $10.6^\circ$  with the  $z$ - $y$  terminator plane. The relative position of the trajectory vector is defined here such that the vector passes through the  $x$ - $z$  plane at a point defined by  $x_0$  and  $z_0$ , this giving rise to a closest approach distance to the nucleus of  $a_0$ . Although the relative orientation of the trajectory vector is well known, the absolute

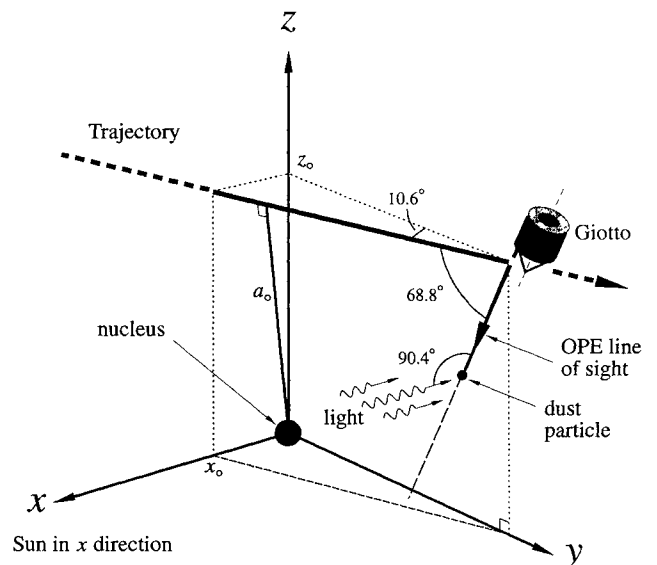


**Figure 1.** Geometry of the *Giotto* Extended Mission flyby with Comet 26P/Grigg–Skjellerup. The orthogonal coordinate system, centred on the nucleus, has the  $x$ -axis pointing towards the Sun, with the  $x$ - $y$  plane parallel to the spacecraft’s relative velocity vector. *Giotto*’s spin axis was almost parallel to the  $y$ - $z$  plane and at an angle of  $68.8^\circ$  to the velocity vector. The solar phase angle of dust particles in the OPE line of sight was therefore  $90.4^\circ$ . The location of the nucleus relative to the trajectory is defined by the parameters  $x_0$  and  $z_0$  which may have been positive or negative.  $a_0$  indicates the closest approach distance of the spacecraft to the nucleus.

position is not determined, i.e. the values of  $x_0$  and  $z_0$  are unknown. This is due of course to the absolute position in space of the cometary nucleus being unknown (as opposed to uncertainty in *Giotto*’s trajectory). However, to aid visualization (and for the purposes of the modelling presented later), it is easier to maintain our reference frame on the nucleus and try to determine likely values of  $x_0$  and  $z_0$ . The OPE telescope was situated near the outer edge of the ‘rear’ of *Giotto*, and the line of sight was parallel to the spacecraft’s spin axis (where the spin axis was almost parallel to the  $z$ - $y$  terminator plane). Note that the phase angle of  $90.4^\circ$  for sunlight being scattered from a dust particle in the OPE line of sight is maintained throughout the near-nucleus encounter.

It is clear from the geometry shown in Fig. 1 that the location of the path of *Giotto* with respect to the nucleus would make a crucial difference to the gathered experimental data. With positive values of  $z_0$  and near-zero values of  $x_0$ , then the nucleus could appear in the OPE line of sight. Alternatively, if  $z_0$  were significantly negative, then OPE would never sample the near-nucleus region.

At the Halley flyby the targeting of the spacecraft was aided by the ‘pathfinder concept’, using imaging from the *VEGA* missions several days before to reduce the uncertainties in the nucleus position. Subsequent determination of the flyby distance was performed using HMC imaging. Neither technique was possible at the Grigg–Skjellerup flyby since it was the only spacecraft and the HMC was inoperable. The estimated targeting uncertainty pre-encounter was around 200 km (1 sigma; T. A. Morley, personal communication), the targeting being at the nominal nucleus position.

Three large impacts were detected by DIDSY, indicating that the mass loss is dominated by large particles as at Halley (McDonnell et al. 1993). This low detected fluence, owing to the combination of low cometary activity, low flyby velocity and the tilt of the *Giotto*

**Table 1.** The OPE filters.

Filter	$\lambda_0$ (nm)	FWHM (nm)
OH	310	6.0
<sup>1</sup> CN	390	4.0
<sup>1</sup> C <sub>2</sub>	515	4.0
<sup>2</sup> CO <sup>+</sup>	425	4.0
‘Blue’ Dust	442	4.5
‘Green’ Dust	577	10.0
<sup>3</sup> ‘Red’ Dust	717	3.5

Notes: <sup>1</sup>CN and C<sub>2</sub> channels multiplexed. <sup>2</sup>CO<sup>+</sup> channel did not have polaroid foils. <sup>3</sup>No useful data owing to a loss in sensitivity after Halley encounter.

bumper shield to the relative velocity, places only poor constraints on the nucleus miss distance (approximately 50 to 1000 km depending on the nucleus model parameters). However, since OPE was sensitive to all scattering particles along a line of sight passing right through the coma, the shape of the brightness profile provided the possibility of a reasonable determination of the miss distance.

### 3 OPE

#### 3.1 The instrument

To constrain models describing the physical properties of the dust, OPE was chosen to measure the brightness at various wavelengths and states of polarization. To guarantee its reliability, the polarimeter was designed with no moving parts. Imaging was performed through a mosaic of interference filters (which were arranged in such a way so as to compensate for chromatic effects) placed in front of the objective lens of the refracting telescope. By imaging on to a microchannel plate, spectral discrimination could be achieved. A polaroid foil, placed on all filters but one, allowed the polarization to be determined as the analyser turned along with the spinning spacecraft. The resulting instrument was light (1.3 kg) with an undemanding power consumption (1.1 W) as required on an interplanetary space vehicle (Levasseur-Regourd et al. 1986a).

OPE was located on the rearward-facing platform of the spacecraft (relative to the motion of the probe at the Halley encounter). A single stage cylindrical baffle was designed to minimize light scattered from the rear of the antenna and tripod. A baffle cover holding a tritium-phosphor calibration source (later released by firing a pyrotechnic device) avoided contamination of the optics during launch and allowed the sensitivity of the instrument to be checked prior to launch and in space before the Halley encounter. The objective lens was used to image the light from the comet on to a field stop, providing a 2°62 field of view. The mosaic was imaged on to the photocathode of the microchannel plate photomultiplier by a field lens behind the field stop. Photoelectrons generated at the photocathode were amplified and focused to an anode segment corresponding to a single filter and thus a distinct channel (Giovane et al. 1991).

The polarized components of the light were measured in seven bandpasses or channels, ranging from the near-ultraviolet to the near-infrared. Three channels, the so-called blue, green and red channels, were devoted to the observation of the scattering of solar light by cometary dust grains, in emission-free continuum bands (see Table 1).

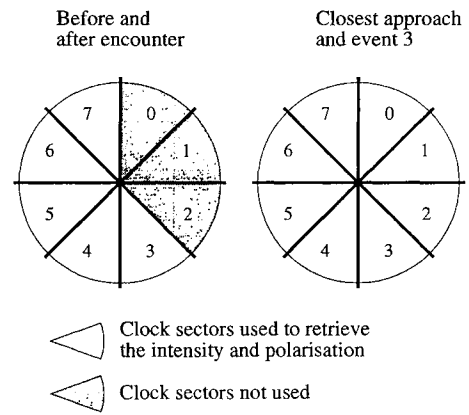


**Figure 2.** OPE clock sectors used during the encounter. Eight sectors were sampled during one spacecraft revolution (lasting 4 s). Sectors 0, 1 and 2, however, were contaminated with stray light (thought to be from the antenna dish) and so were not used, except when the signal levels were high enough such that the contamination did not dominate (i.e. near closest approach and event 3). Polarization pairs were calculated from sectors (0,2), (1,3), (2,4), etc.

Four other channels, the so-called OH, CN, C<sub>2</sub>, and CO<sup>+</sup> channels (with no polaroid foil in front of the CO<sup>+</sup> filter), were devoted to the observation of light emitted by cometary gases. During a spacecraft spin period (of ~4 s), eight consecutive measurements of the polarized brightness,  $Z_i$ ,  $Z_{i+1}$ ,  $Z_{i+2}$  etc. (each of them integrated over a 45° rotation of approximately ~0.5 s), were performed in eight clock sectors, simultaneously for the seven channels. Fig. 2 illustrates the clock sectors.

#### 3.2 Data reduction procedure

The polarized light intensity can be retrieved from the measured signals, by removing the average dark count (smaller than 5 counts per half second interval in the blue and the green channels), then removing the astronomical background and finally applying the absolute calibration factor. These contributions were estimated for all the clock sectors of each channel and did not significantly change from before to after encounter. The appropriate values for each filter were subtracted from all the data.

The total intensity  $Z_{\text{tot}}$  was obtained by adding two perpendicularly polarized components i.e.

$$Z_{\text{tot}} = Z_i + Z_{i+2}, \quad (1)$$

where  $Z_i$  is the polarized intensity on clock sector  $i$  (see Fig. 2). The polarization  $P$  is obtained by

$$P = \frac{2\sqrt{(Z_i - Z_{i+2})^2 + (Z_{i+1} - Z_{i+3})^2}}{(Z_i + Z_{i+2}) + (Z_{i+1} + Z_{i+3})}. \quad (2)$$

The polarization measurement uses intensities taken from four consecutive clock sectors, these data being gathered over half a spacecraft spin period i.e. 2 s. It should be noted, however, that during this period some variation in intensity may occur owing to the changing field of view as *Giotto* travels through the coma as well as the changing polarization itself. To minimize this potential source of error the data from the CO<sup>+</sup> channel, which is unpolarized and dominated by dust scattering in the inner coma, is used to normalize the intensity changes for each rotation before the polarization is calculated.

As the rotation of the spacecraft (which defines the sector positions) is continuous, the polarized intensity for each sector

**Table 2.** Background intensity components of the OPE blue, green and red channels. Because of the higher sensitivity of the green channel, counts obtained in the blue channel are a factor 0.46 that of the green channel. The red channel suffered a drastic loss of sensitivity during the Halley encounter.

Channel	Background signal (counts, DC removed)	Response ( $10^{-7} \text{ W m}^{-2} \text{ sr}^{-1} \mu\text{m}^{-1} \text{ ct}^{-1}$ )	Pre-launch estimate
Blue	$26^{+4}_{-10}$	$2.6 \pm 1.3$	2.09
Green	$56^{+4}_{-20}$	$1.2 \pm 0.6$	0.88
Red	$02^{+6}_{-10}$	$\sim 24$	4.40

position is a sum over a  $45^\circ$  sector rather than measured at a single position as would occur in conventional polarimeters. The maximum underestimation of the true polarization would occur when the polarization vector is aligned exactly with one of the sectors. However, even in this case the measured value would be 0.975 times the true value.

During the flyby, all the housekeeping data (high voltage, low voltage, temperature) remained nominal. A few telemetry losses took place during the flyby, and a few suspect data points, probably arising from telemetry faults, were removed. Near closest approach,

data corresponding to one spin period were lost, most likely because of instrumental effects on the spacecraft radio system, immediately before a slight nutation was noticed and dust impacts were recorded (Pätzold et al. 1993; McDonnell et al. 1993).

OPE had remained operational after the Halley flyby, as demonstrated during the 1990 April and 1992 June tests. However, a stray light contamination, which was almost certainly due to solar light scattered from the despun antenna during part of the *Giotto* rotation and which reached 300 counts per half second interval for the blue channel, was seen on clock sectors 0, 1 and 2 (Fig. 2). The intensity

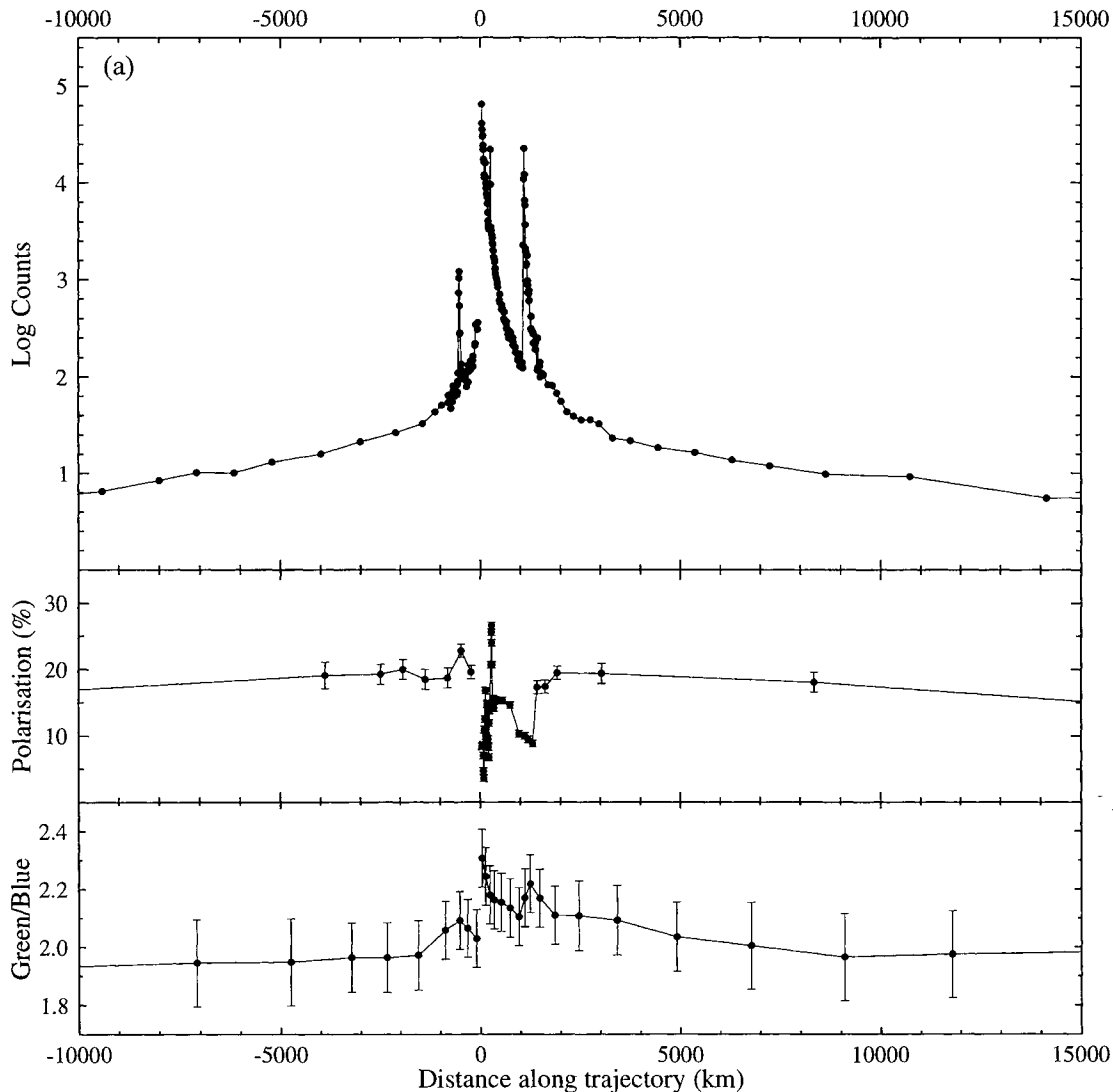


**Figure 3.** (a) Upper panel: OPE data in the green (577-nm) channel ( $-10\,000$  km to  $+15\,000$  km is shown). Counts per second are shown calculated for the polarized sector pairs (see text). Middle panel: polarization. Lower panel: ratio of green- to blue- (442-nm) channel data. (b) As in (a) but for  $-750$  km to  $+1750$  km.

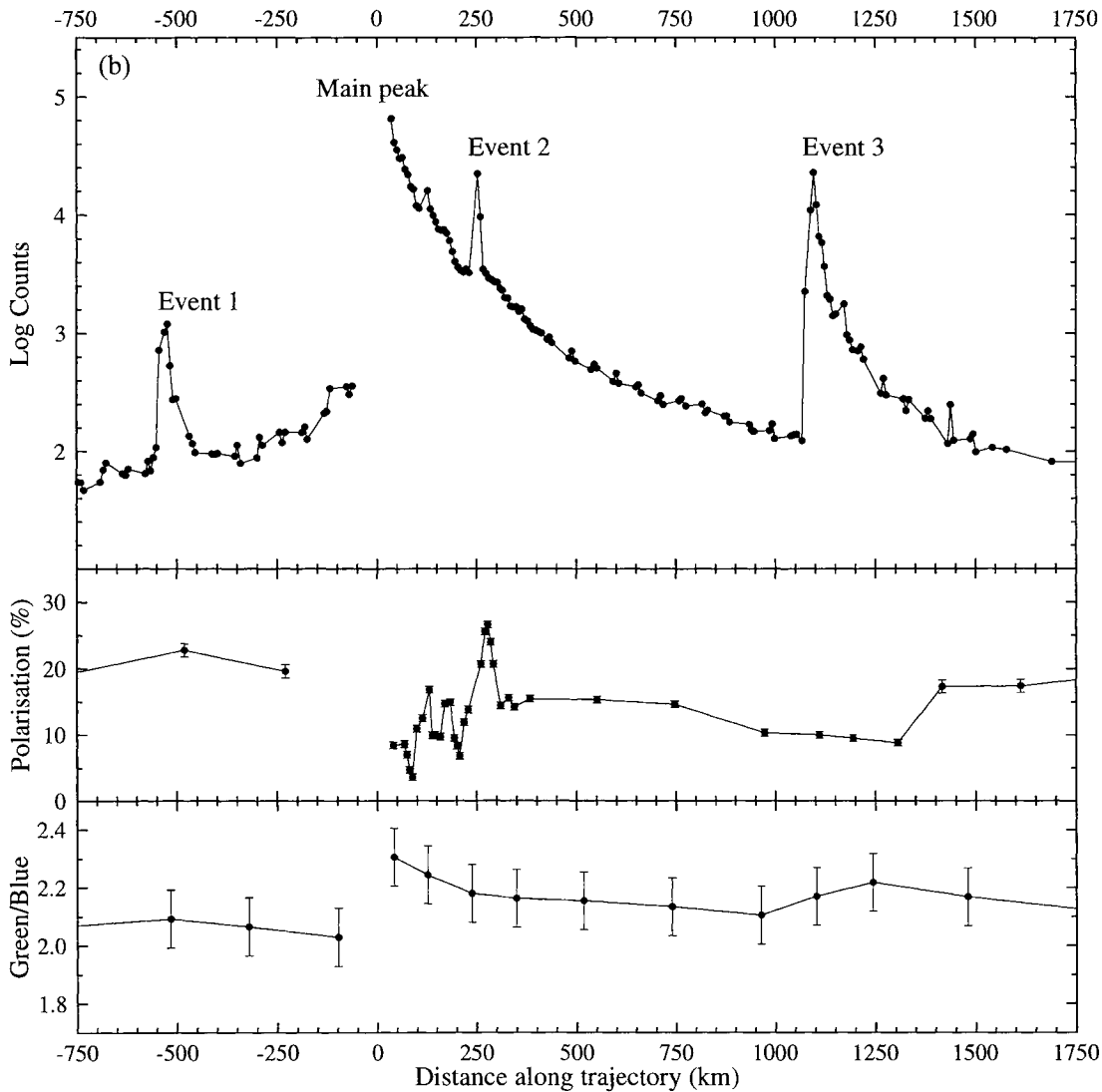


Figure 3 – continued

was therefore computed only three times per rotation of the spacecraft, spaced at 0.5-s intervals, from the combination of the polarized brightness in clock sectors (3,5), (4,6) and (5,7). The polarization was retrieved once per rotation, from the combination of polarized brightness in clock sectors 4, 5, 6 and the mean of sectors 3 and 7. During closest approach, however, all the clock sectors could be used because of the high level of the signals, so obtaining more continuous intensity and polarization data sets.

### 3.3 Sensitivity and calibration at the Grigg–Skjellerup encounter

As a result of the absence of the on-board calibration lamp after the baffle was fired prior to the Halley encounter, the sensitivity had to be checked through observations of the astronomical background in the field of view of the instrument. This background is built up of three components: (1) the zodiacal light from solar light scattered by interplanetary dust which (along with planetary light) produces the Solar system component; (2) stellar light scattered by interstellar dust which (along with the light from stars) produces the diffuse Galactic component; (3) the very faint extragalactic component.

Prior to the Grigg–Skjellerup flyby, an OPE calibration test was

performed. The *Giotto* spin axis was such that the OPE line of sight was pointing to a field in Sagittarius with right ascension  $19^{\text{h}}21^{\text{m}}$  and declination  $-22^{\circ}06'$  (Morley 1991). The helioecliptic coordinates were  $(\lambda - \lambda_{\odot}) \sim 90^{\circ}$ ,  $\beta \sim 0^{\circ}$ , i.e. the observations were made in the vicinity of the ecliptic plane, at  $90^{\circ}$  from the Sun. The Galactic coordinates were  $l = 16^{\circ}$ ,  $b = -17^{\circ}$ , i.e. the observations were reasonably close to the Galactic plane. From the determination of the zodiacal light component (see the table published in Levasseur-Regourd & Dumont 1980), the estimation of integrated starlight (Roach & Gordon 1973) and the general trend of the diffuse Galactic and extragalactic components (Toller 1990), the total background is computed to be equal to  $530 \pm 70 S_{10(V)}$  (a unit of  $S_{10(V)}$  being the equivalent number of tenth visual magnitude solar-type stars per  $\text{deg}^2$ ). This corresponds to  $6.7 \pm 0.9 \times 10^{-6} \text{ W m}^{-2} \text{ sr}^{-1} \mu\text{m}^{-1}$  for the blue and the green channels and  $4.8 \pm 0.7 \times 10^{-6} \text{ W m}^{-2} \text{ sr}^{-1} \mu\text{m}^{-1}$  for the red channel.

The background brightness detected prior to and after the Grigg–Skjellerup flyby, produced from the combination of two clock sectors free of stray light contamination, is given in Table 2, together with the resulting sensitivity. The ratio of the signals from the blue and the green channels is  $\sim 0.46$ . This value is consistent with the estimated pre-launch sensitivities (Giovane et al. 1991), indicating

**Table 3.** The OPE data for the green (577-nm) channel.  $d$  equals distance along the trajectory from the nominal assumed peak (at 15:30:45 GRT). Counts are number  $s^{-1}$ . The blue-channel data follow the same general form. (For example in the  $d = \pm 1000$  km region, the blue counts are a factor  $\sim 0.47$  lower than those for the green.)

$d$ (km)	Counts								
-19754	1	-404	95	204	3617	656	366	1264	310
-17433	1	-398	96	211	3393	663	312	1271	414
-15566	3	-355	91	218	3276	706	269	1277	301
-13643	3	-349	113	225	3469	712	296	1320	279
-11323	5	-341	79	232	3246	719	249	1327	222
-9408	7	-300	88	253	22168	759	268	1334	274
-8003	8	-293	132	260	9585	764	280	1375	191
-7078	10	-286	113	267	3472	776	242	1382	221
-6153	10	-244	145	274	3203	817	251	1389	189
-5210	13	-237	119	281	2920	825	212	1431	116
-3993	16	-230	145	288	2830	831	223	1438	249
-3002	21	-188	145	295	2712	873	199	1446	124
-2109	26	-181	162	302	2682	879	200	1488	128
-1438	33	-175	127	309	2387	886	177	1494	140
-1130	43	-132	210	315	2298	936	169	1501	99
-963	51	-126	219	322	1994	941	152	1543	108
-795	54	-118	341	329	1977	947	147	1578	103
-789	64	-76	353	336	1698	986	150	1690	82
-746	55	-70	304	343	1665	993	171	1802	81
-740	55	-62	358	350	1675	999	128	1914	67
-733	47	36	64757	357	1524	1040	135	2024	55
-691	55	43	40828	364	1598	1047	138	2164	43
-683	70	50	35349	371	1307	1054	139	2331	39
-677	80	57	29990	378	1261	1068	123	2527	36
-635	65	64	30608	385	1147	1075	2255	2750	36
-627	63	71	24316	392	1072	1089	10883	2974	32
-621	71	78	21947	399	1052	1096	22669	3309	23
-578	65	85	17430	406	1029	1103	12129	3755	22
-572	83	92	16472	413	1003	1110	6575	4450	18
-565	69	99	11983	427	889	1117	5850	5374	16
-558	89	106	11336	433	924	1124	3686	6299	14
-551	108	127	16002	439	832	1131	2086	7242	12
-544	722	134	11191	482	612	1138	1944	8629	10
-530	1030	141	9849	489	703	1145	1402	10731	9
-523	1202	148	8727	497	578	1152	1453	14148	6
-516	534	155	7596	537	491	1173	1765	18762	6
-509	276	162	7453	545	545	1180	966	23488	4
-502	280	169	7501	552	505	1187	872	29298	3
-468	135	176	7011	593	391	1194	720	37003	3
-460	117	183	6076	601	459	1207	711	48780	1
-454	98	190	4890	607	377	1215	768	62905	1
-412	95	197	4024	650	351	1221	603	76974	1

little relative change in the behaviour of the green and the blue channels. The red channel, however, suffered a drastic loss of sensitivity during the Halley encounter. We present here, therefore, only results for the blue and the green dust continuum channels.

#### 4 GRIGG-SKJELLERUP FLYBY DATA

Data from the blue and the green channels follow almost identical trends and for subsequent modelling we have simply used the green (577-nm) channel as this receives more counts (owing to the higher sensitivity as discussed above). All data are given as a function of distance,  $d$ , along the *Giotto* trajectory with zero denoted by the estimated time of the maximum intensity, which we take to be 15:13:45 Ground Received Time (GRT). The green intensity data are plotted in Fig. 3(a), for the range  $d = -10\,000$  to  $+15\,000$  km, together with the polarization and the colour ratio green/blue. The

actual data values are tabulated in Table 3 for the range approximately  $d = -20\,000$  to  $+77\,000$  km. Where possible, individual intensity ( $Z_{\text{tot}}$ ) values are given (generally where the signal is highest; in the innermost coma) although values are averaged (to increase the signal-to-noise ratio) where count rates were low (generally when  $|d| > 1000$  km) using between 1 and 200 rotations depending on the signal. The brightness is given as an instrumental count, as the calibration discussed above is tentative.

Fig. 3(b) shows the data for the innermost coma from  $d = -750$  km to  $+1750$  km. We have labelled the main peak and three main ‘events’. Note the data dropout near the 0-km region. It is likely that the peak OPE brightness occurred in this dropout region, and it is here that we have chosen the  $d = 0$  position, at 15:13:45 GRT. This choice is of course arbitrary. The true closest approach time is likely to be somewhat different from this, and in fact the peak signal might be due to another ‘event’ with the peak in brightness resulting from

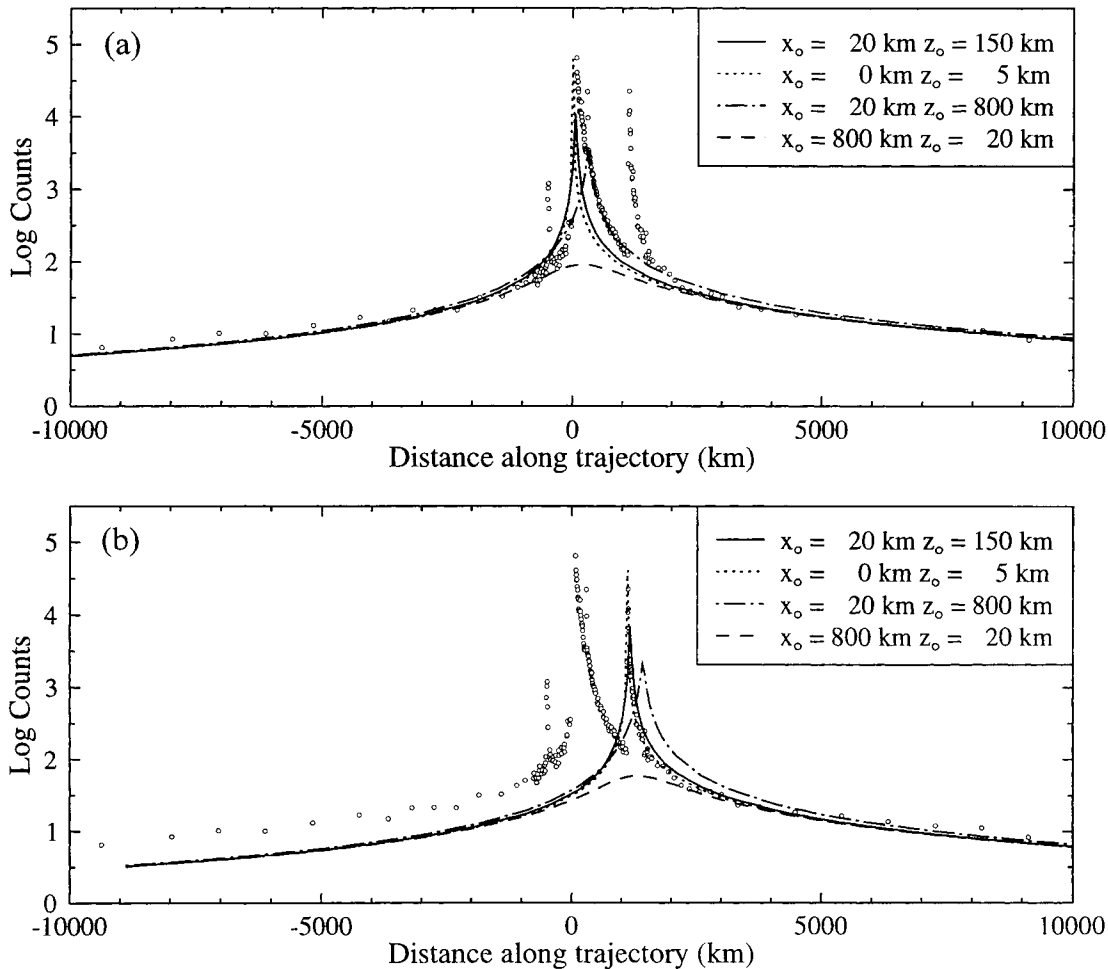


**Figure 4.** Overall coma dust models compared with data. (a) Fits assuming the coma dust spatial density obeys a simple  $r^{-2}$  law ( $r$  being cometocentric distance). (b) Fits assuming event 3 is a ‘main peak’.

the cometary coma occurring later. This however does not affect the subsequent modelling in this paper as the exact relative position of the nucleus is a free parameter.

First inspection of the inner coma data (Fig. 3b) reveals that the data are significantly asymmetric around the closest approach point. Post-encounter shows a pronounced brightening compared to pre-closest approach. For pre-closest approach, the form of the data approximates to a  $d^{-1}$  power law (i.e. counts proportional to  $d^{-1}$ ) for at least  $-10\,000$  km to  $-1000$  km. This  $d^{-1}$  relation is also seen post-encounter at distances greater than about  $+3000$  km, although for  $d < +3000$  km (post-closest approach) the form of the data follows more closely to a  $d^{-1.7}$  relationship (as was noted in Lvasseur-Regourd et al. 1993a). Note that this refers only to the general trend of the data, and one should be careful when making immediate conclusions as to the variation of spatial dust density in the cometary coma. If considering the integrated brightness contribution from a cylindrical volume around a line of sight viewed through the entire coma, a  $d^{-1}$  relationship would be indicative of a  $r^{-2}$  (spherically symmetric) dust spatial density relationship (where  $r$  is the distance from the nucleus). However, as *Giotto* was passing through the coma (and not necessarily directly bisecting a spherically symmetric cloud), the brightness contribution in the OPE conic field of view cannot be taken to be a simple cylindrical contribution, and thus the peak intensity may not correspond to the closest approach point. For example, for an encounter geometry

such that  $x_0 = 0$  km and  $z_0 = 200$  km (i.e.  $a_0$  is also 200 km), a passage through a spherically symmetric coma would yield the peak intensity at  $\sim 5$  s after the closest approach point.

Although the asymmetry in the data is clearly significant perhaps the most striking features are the ‘spikes’, which we have labelled as events 1, 2 and 3 in Fig. 3(b). The approximate  $d^{-1.7}$  relationship that the data show in the  $d < 3000$  km post-closest approach region does not necessarily indicate a departure from a  $r^{-2}$  dust spatial density as the presence of these spike events shows that some activity or artefacts may be superimposed on a background  $r^{-2}$  coma. An in-depth discussion of possible explanations for the data profile is given in the following sections.

The polarization data are also shown in Fig. 3. The solar light scattered by cometary dust is linearly polarized. The degree of polarization depends upon the phase angle between the Sun and the observer as seen from the scattering dust particle, and the location within the coma. When considering whole-coma observations (see Lvasseur-Regourd, Hadamcik & Renard 1996), all comets exhibit similar phase curves with a maximum polarization ( $P_{\max}$ ) occurring near a  $90^\circ$  phase angle. However, a  $P_{\max}$  of around 25 per cent is noticed for comets such as 1P/Halley, whereas a value below 15 per cent is obtained for relatively inactive comets (Lvasseur-Regourd 1992; Lvasseur-Regourd et al. 1996). Polarization maps of the coma, as compared with brightness maps, enhance some details; jets are revealed by an increase in polarization (e.g. Eaton, Scarratt

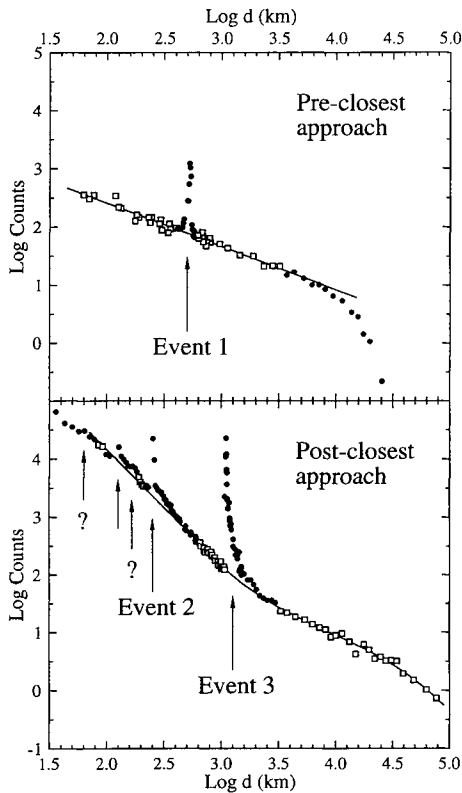


**Figure 5.** Intensity as a function of distance from encounter for the green dust channel. The three main events are labelled, with possible secondary peaks also indicated with arrows. The open symbols represent the data for which the fits to the ‘background’ (or, more correctly, the underlying trend in the data) have been made.

& Warren-Smith 1988); a circumnucleus halo extends to nucleus distances of  $\leq 2000$  km where a decrease in polarization is observed (Renard, Lvasseur-Regourd & Dollfus 1992; Renard, Hadamcik & Lvasseur-Regourd 1996). A change in the value of  $P_{\max}$ , as well as

an increase or decrease at a given phase angle, is likely to be due to a change in the physical properties (e.g. size distribution) of the scattering dust.

During the Grigg–Skjellerup flyby, the phase angle remained constant at  $90.4^\circ$ , i.e. in the phase range where the polarization reaches its maximum  $P_{\max}$ . The polarization beyond 10 000 km from the comet is around 15 per cent, consistent with the typical values for low-activity comets. Drastic changes take place closer to the nucleus (Fig. 3b). A sharp *increase* is correlated with event 2, and a smaller increase with event 1 (apparent even in the smoothed data shown in Fig. 3b). However, a significant *decrease* in polarization occurs at the main peak, and in the region of event 3.

The colour data, also shown in Fig. 3, show that the blue and the green channels remain virtually identical for most of the encounter, with a colour ratio that remains generally constant after the absolute calibration is taken into account. A slight reddening is apparent in the inner coma, for distances to the nucleus smaller than 5000 km, and such an effect was observed for Comet Halley (Lvasseur-Regourd et al. 1986b), and may indicate a change in the physical properties of the grains in this region.

In this paper we are concerned principally with the explanation for intensity variations in the inner coma, and in particular the OPE events. In order to explain these events as real cometary phenomena we must investigate the expected properties of a ‘normal’ coma, and investigate any possible instrumental or spacecraft-related effects.

## 5 GENERAL DUST COMA MODELS

A cometary dust coma density distribution depends on the total dust production rate, its variation with time and the position of active regions on the nucleus surface, and the dust grain size distribution and composition which determine the ratio of radiation pressure to gravitational forces ( $\beta$ ). The most trivial model would be a uniform and isotropic emission of grains with  $\beta = 0$ , resulting in an inverse square law fall-off in the dust spatial density. The fountain model (Divine 1981, 1983, 1985) provides a more realistic representation, but requires a number of nucleus and dust properties as input

**Table 4.** Properties of the OPE events. The contrast with the background is the factor by which the event peak appears to exceed the local background as shown in Fig. 5.

Event	1	Main	2	3
Peak intensity (counts $s^{-1}$ in green)	$\geq 1130$	$\geq 65000$	$\geq 19900$	$\geq 22500$
Contrast with background	15	—	9	185
Ground Received Time	15:30:07	15:30:45	15:31:03	15:32:03
Distance $d$ from main peak (km)	−525	0	250	1095

**Table 5.** Time line of events at 26P/Grigg–Skjellerup encounter. Note the OPE events do not coincide with the DIDSY events, although the telemetry drop-out and the OPE brightness peak do appear to be correlated with the GRE impact event.

Time (GRT)	Dist $d$ along trajectory (km)	Event	Polarization	Comment
15:30:07	−525	OPE event 1	~25 per cent	
15:30:43	−30	GRE impact		‘Whopper’ $\geq 30$ mg
15:30:43–47	−30 to 30	Telemetry loss		All instruments
15:30:45±2	0	OPE max. brightness	< 10 per cent	
15:30:48–51	40–85	DIDSY impact		‘BigMac’ $100^{+100}_{-60}$ $\mu$ g
15:30:51–54	85–125	DIDSY impact		‘Barley’ $2^{+4}_{-1}$ $\mu$ g
15:31:03	250	OPE event 2	~25 per cent	
15:31:31–32	645–660	DIDSY impact		‘Bretzel’ $20^{+25}_{-10}$ $\mu$ g
15:32:03	1090	OPE event 3	~10 per cent	

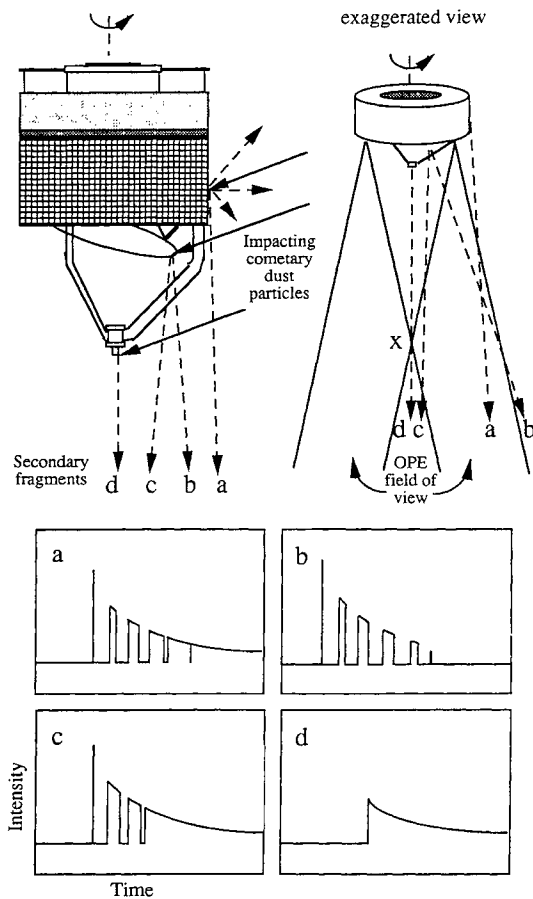


**Figure 6.** Schematic of trajectories of ejecta from impacts of cometary dust on *Giotto*. The conical field of view of OPE with half angle  $1.3^\circ$  rotates with a period of 4 s. a, b, c and d are spherical ejecta which can enter the OPE field of view which would produce lightcurves as shown (in reality these would be sampled eight times per revolution as described in the text). The point X lies  $\sim 43$  m from the spacecraft. Particles d and c must be produced by impact events on the antenna dish and the tripod struts.

parameters which for any given comet may be poorly understood or unknown. It has, however, provided a powerful tool for predicting the average coma properties for comets including Halley (Pankiewicz 1989; Pankiewicz et al. 1989).

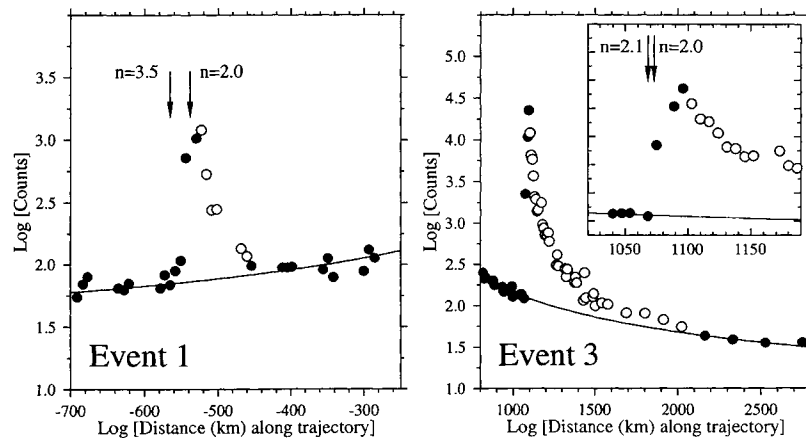


**Figure 7.** Profiles of events 1 and 3. The white filled circles indicate the points assumed to be part of the decay of the event profiles. By subtracting the underlying local background (shown here as the solid curves; as shown in Fig. 5) we can fit the profile decrease to a  $|d - d_0|^n$  power law where  $d_0$  is the assumed start of the 'impact event'. The arrows indicate the position of  $d_0$  corresponding to the value of  $n$  as labelled.

Once a coma spatial density model has been produced, the observed intensity can be derived by applying a dust scattering model (Goidet-Devel 1994; Goidet-Devel et al. 1997) and integrating along the OPE line of sight as a function of time using the flyby geometry as shown in Fig. 1. When doing this one must remember that the effective viewing area of OPE must be treated as a cone rather than a cylinder.

Fig. 4 shows fits to the data assuming a simple  $r^{-2}$  relationship for dust particle spatial density (i.e. spherically symmetric coma), with various flyby geometries as described by  $x_0$  and  $z_0$ . The main peak is fitted in Fig. 4(a) and the outer coma is reasonably 'well-behaved', fitting quite well to a simple  $r^{-2}$  spherically symmetric dust density. The fits are (as expected in the outer coma) not significantly dependent on the inner coma flyby geometry. The inner coma however is clearly complex and needs more in-depth modelling. In Fig. 4(b) the curves have been separately fitted to event 3, as if this was the main peak (i.e. the centre of a spherical coma). It is clear that the fit is not good, and that event 3 is indeed a feature superimposed upon the main activity curve, the cause of which needs to be explained.

## 6 OPE EVENTS

Before considering possible explanations for the OPE events, it is worth looking at their characteristics in more detail. Fig. 5 illustrates the three main events as well as several others, together with fits to the nominal background intensity. For the background near events 1 and 2, power-law fits are appropriate:

$$\text{background count near event 1} = 7885|d|^{-0.745},$$

$$\text{background count near event 2} = 1.447 \times 10^8 |d|^{-2.0},$$

whereas higher order terms are needed for event 3:

$$\log_{10}(\text{background count near event 3}) = 26.77 - 17.73 \log_{10} d + 4.25(\log_{10} d)^2 - 0.36(\log_{10} d)^3.$$

The intensities of each event can then be obtained simply by subtraction of the calculated local background at each point. The basic properties of the three main events are listed in Table 4.

The shapes of the event profiles provide evidence for their origin. Instrumental effects would manifest themselves as either a discontinuity or drift in signal, or if an intermittent effect, a rapid rise and an exponential fall. The flawless stability of the house-keeping data (high voltage, low voltage, temperature) during the

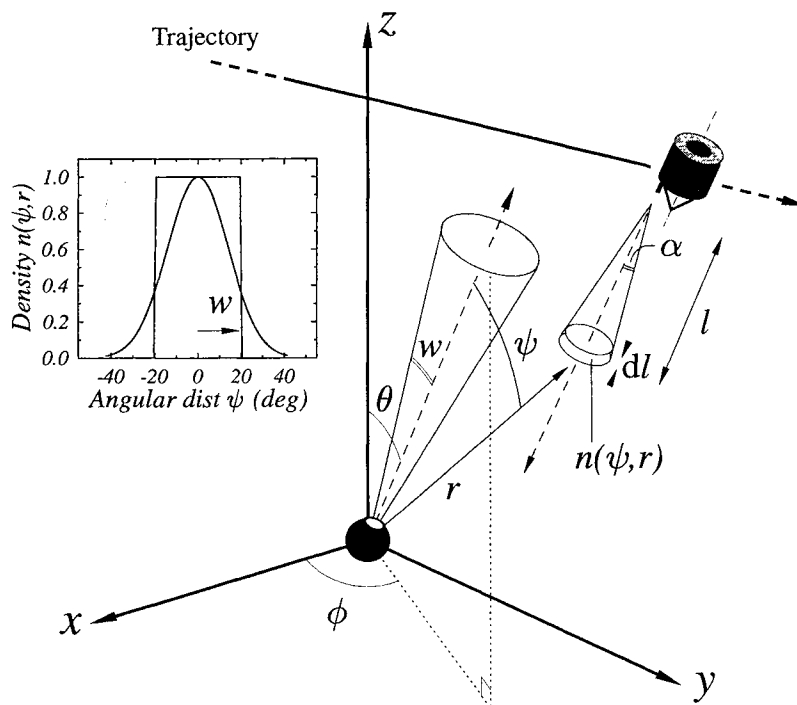


**Figure 8.** Schematic of the jet model. Particles in jets are assumed to be emitted radially. A jet is defined by parameters  $f$ , the fraction of total dust emission from the comet emitted in the jet, and  $\omega$ , the angular half-width of the jet (see text). The dust spatial density  $n(\psi, r)$  at cometocentric distance  $r$  at an angular distance  $\psi$  from a jet goes to contribute to the observed brightness seen in the OPE conic field of view.

flyby, and of the background signals before and after the flyby, rules out an electronic failure. In addition, event 3 does not exhibit an exponential decay and the time constants for events 1 and 2 are different.

Optical artefacts because of the damage caused at the Halley encounter can also be ruled out. Since the OPE telescope points along the central axis of the spacecraft which is aligned with the velocity vector, celestial sources would not move in the field of view. Reflection of sunlight from the spacecraft structure would be modulated with the spin period and is the likely cause for the high background signals in three sectors. In order to obtain a changing signal (events) either the source or the reflecting material must move. In either case, however, the reflection would still be modulated by the spin.

Individual cometary dust grains passing close to the spacecraft and through the OPE line of sight could produce a large signal which would decay with time. However, in order to produce a sufficiently large signal, a dust grain would have to be close to the spacecraft and hence would not remain in the line of sight for long enough as a result of the oblique angle at which the particle would enter the field of view. In order to be visible for a number of seconds, the object would have to be distant and therefore large. In this case the relative change of distance as the particle passed through the field of view would be small giving a negligible decay in brightness.

In the case of event 3, with a duration of  $\sim 100$  s, the distance traversed in the field of view will be  $\sim 1400$  km and hence the distance of an object from *Giotto* would need to be 28 000 km. Assuming a lambertian sphere with geometric albedo of 0.04, a particle size of  $\sim 9$  km is required to provide the observed peak signal, but the profile shape would be virtually flat. It is clear that individual cometary particles cannot reproduce the properties of the observed events.

## 7 IMPACT ON *GIOTTO* AS AN EXPLANATION FOR EVENTS

The impact of cometary dust particles on *Giotto* seriously affected the performance of a number of instruments at the Halley flyby. We now investigate the possible explanation of the OPE events as a consequence of such impacts during the Grigg–Skjellerup flyby.

Although only three impacts were detected by DIDSY, this experiment was located on the bumper shield, which at the Grigg–Skjellerup flyby was inclined at an angle of  $68^\circ 8'$  to the relative velocity vector. It presented a cross-sectional area of  $\sim 0.76 \text{ m}^2$  compared with  $\sim 3.6 \text{ m}^2$  for the whole spacecraft (McDonnell et al. 1993). The largest impact on the spacecraft, coinciding with the telemetry loss near closest approach, occurred on the rear of the spacecraft, as derived from the *Giotto* Radio Science Experiment (GRE) data (Pätzold et al. 1993). It is therefore possible that some effect of impacts or their resultant plasma and debris could be responsible for the other events seen by OPE. DIDSY and GRE data allow us to estimate the mass of the largest impacting particles.

The times of the DIDSY impacts were known to an accuracy of  $\sim 3$  s or better but did not coincide with OPE events (see Table 5). However, if the events are related to impacts, then those hitting near the OPE experiment (and therefore not detectable by DIDSY) are likely to have the maximum effect. Unfortunately, moderate-sized impacts near the rear of the spacecraft would only be detectable if they caused significant velocity or nutation shifts in the spacecraft's motion. The mass of the largest impact, near closest approach, was 30 mg or greater (Pätzold et al. 1993). It dominated the total mass influx to the spacecraft and was consistent with the mass distribution index for the DIDSY impacts (McDonnell et al. 1993). This implies a total of  $\sim 15$  impacts of particles with mass in the range

1  $\mu\text{g}$  to 1 mg and only one with mass  $> 1$  mg on the whole spacecraft during the flyby. We must estimate effects of such impacts to determine if they are a possible source of the events seen in the OPE data.

An impact of a particle at  $14 \text{ km s}^{-1}$  on to a semi-infinite target will vaporize the particle and a considerable mass of target material. The total charge liberated from a  $1 \mu\text{g}$  impact will be a few  $\mu\text{C}$ , and from a 1 mg impact a few mC (see e.g. Kruger 1984). The impact itself would produce an effectively instantaneous optical flash, and the local plasma density would decay with a time constant of much less than a second. It is difficult to conceive of a plasma mechanism which could produce the observed event signals from OPE since the decay of the events is much longer than this.

If a small object passed through the field of view at a very shallow angle relative to the line of sight and at a low relative speed to the spacecraft it might be possible to produce the observed brightness decay seen in the OPE events. This might be envisaged if an impact on the side of the spacecraft produced a small secondary fragment or cloud of particles (as suggested by Le Duin et al. 1996). However, the line of sight is hardly accessible to impacts on the majority of the surface of the spacecraft. In almost all of these cases, the ejecta would pass in and out of the field of view rapidly once, or several times owing to OPE's position offset from the spin axis of *Giotto*. Any irregular shaped object would produce rapid variations in scattered light as it tumbled. Fig. 6 shows the geometry and expected brightness profile of a spherical object as a function of time. The probability of obtaining secondary ejecta in the field of view, from three separate impacts of type d but none of types a, b or c, large enough to produce signals between 10 and 200 times the cometary brightness, in such a geometry that the OPE sampling produced a smooth intensity decay with time, is very low.

Consider also the profiles of the event data. If a spherical, or non-spinning, ejecta particle (produced by an impact event) travelled away from *Giotto* down the OPE line of sight at a constant relative velocity with respect to the spacecraft, the apparent brightness of the particle, as seen from *Giotto*, would fall as  $t^{-2}$  where  $t$  is the time from the impact event. This means that the background-subtracted profiles of the events seen in the OPE data would fall as  $|d - d_0|^{-2}$  where  $d$  is the distance along the OPE trajectory (as in Fig. 3) and  $d_0$  is the distance along the trajectory at which the impact occurs. This condition also holds if we have many particles, perhaps constituting an ejecta cloud, travelling down the line of sight, even if they have different (but constant) individual velocities. However, the value of  $d_0$  is unknown, and its assumed position significantly affects the form of the profile decay derived from the data.

We can investigate whether a  $|d - d_0|^{-2}$  behaviour is seen in the data. We will consider events 1 and 3 only, as events near the main brightness peak may be convolved with other events, i.e. event 2 cannot be background-subtracted unless one makes initial assumptions about what convolved events exist in the complex main-peak region.

Fig. 7 shows in detail the data around events 1 and 3. The solid curve shows the assumed background (as in Fig. 5) which can be subtracted from the data points. We identify the data points we consider to be part of the event decay, i.e. where the ejecta is fully within the OPE field of view (open circles in Fig. 7). We can then pick an arbitrary  $d_0$  to indicate the start of the event (i.e. the point at which the ejecta particle, or *particles*, leave the spacecraft) and plot  $\log[\text{background-subtracted data}]$  against  $\log|d - d_0|$  to investigate the form of the profile decrease. A straight-line fit, with a gradient of  $n$ , would indicate that the event profile decrease varied as  $t^{-n}$ , where

$n = 2$  would be consistent with ejecta travelling down the OPE line of sight at a constant velocity.

On investigation, we find that linear fits adequately describe the data obtained for a range of  $d_0$  values for both events 1 and 3, indicating that the event profiles could indeed decay as  $t^{-n}$ . Strictly speaking, there is only *one* best-fitting power law at any one time, although the data (particularly event 1) are sufficiently noisy that we could realistically fit a variety of  $d_0$  and  $n$  combinations without the quality of fit varying widely. The arrow labelled  $n = 2$  in the event 1 graph in Fig. 7 shows the required position of  $d_0$  needed to obtain  $n = 2$  (the linear fit yielding a regression coefficient of 0.99). However, this nominal 'start of the event' occurs significantly after the apparent rise in the brightness data indicating that this value of  $d_0$  is not realistic. The arrow labelled  $n = 3.5$  shows the position of  $d_0$  which might be chosen as a reasonable position for the start of the event just by inspection, although this  $d_0$  yields  $n = 3.5$  (with a regression coefficient of 0.98) which is inconsistent with the  $n = 2$  requirement of the ejecta scenario. It is worth noting that Le Duin et al. (1996) use data without combining sectors to obtain the true polarized intensity. We have also considered this but find that our conclusions do not change and the profile of the data does not change. It seems then that the profile of event 1 could not be produced by a spacecraft impact.

Consider now event 3. The open circles in the event 3 graph in Fig. 7 show the data points we consider to be part of the decay of event 3. The inset shows the start of the event in detail, showing clearly the non-instantaneous rise of the event. We can perform the same reduction as described above and find the position of  $d_0$  which gives  $n = 2$ , as indicated in the figure by the  $n = 2.0$  arrow. This position occurs *after* the start of the event which is inconsistent with the ejecta scenario. However, by again picking a reasonable position for the start of the event by inspection, we see this start point would yield  $n = 2.1$  as indicated in Fig. 7. Both these fits yielded regression coefficients of 0.99. We investigated the effect of picking slightly different background curves for the background-subtraction of the profiles (for example choosing the ' $r^{-2}$ ' profile for  $x_0 = 20 \text{ km}$  and  $z_0 = 150 \text{ km}$  as shown in Fig. 4a) and we find that the values of  $n$  for a given  $d_0$  vary by up to 0.1 for a range of 'reasonable' backgrounds. We thus conclude that although the  $d_0$  position which produces  $n = 2.0$  for event 3 does occur slightly after the data begin to rise, it is sufficiently close to the start of the event such that a  $t^{-2}$  decay is reasonable. Hence the event 3 profile could be consistent with impact ejecta.

Le Duin et al. (1996) suggested that the *main* brightness peak was caused by a shell of ejecta associated with the GRE ( $\sim 30 \text{ mg}$ ) particle impact (Pätzold et al. 1993), which is thought to have impacted on the side solar arrays near the rear of the spacecraft (i.e. nearest to the antenna tripod structure). The other events were also attributed to impact-related features. Although the profile decay of event 3 was shown above to be broadly consistent with ejecta moving down the OPE line of sight at constant relative velocity, we question the feasibility of this scenario by considering the impact dynamics and geometry.

The shell of ejecta as described by Le Duin et al. (1996) needs to be travelling at a relatively low velocity. Too high a velocity could not produce the long decay seen in event 3, and too low would produce 'flashing' as the ejecta entered the OPE line of sight (see Fig. 6). Le Duin et al. write 'in excess of  $4 \text{ m s}^{-1}$ ', and we calculate of order  $10 \text{ m s}^{-1}$  is needed. However, impact ejecta speeds reflect the hypervelocity nature of the event, with small ejecta particles being closely coupled with the expanding vapour cloud, and travelling with the same velocity as the leading edge of the

vapour cloud (Kadono & Fujiwara 1996). This means that likely lower limits for the ejecta velocity are around twice the impact speed (Eichhorn 1978; Kadono & Fujiwara 1996), which in this case means about  $28 \text{ km s}^{-1}$ . This is clearly not consistent with the impact scenario suggested by Le Duin et al. (1996). However, one can consider spallation in brittle materials (e.g. Asay & Shahinpoor 1993) where a shock wave reflected from the rear surface can cause fracture and cracking of the material at its front surface, producing lower velocity ejecta. Schneider, Stilp & Kagerbauer (1995) note some ejecta velocities produced by this mechanism of around  $0.3 \text{ km s}^{-1}$  by hypervelocity impacts ( $6\text{--}9 \text{ km s}^{-1}$ ) on 14 mm thick panes of quartz glass. These sorts of velocities, although lower than those of the ‘fast’ ejecta, are still too high.

Although the solar array cover glass is a tempting explanation for brittle material spallation products from *Giotto*, the ejecta velocity is not the only problem with the explanation. By virtue of their production mechanism (e.g. Asay & Shahinpoor 1993) spallation products will leave the surface in the direction of the surface normal. This means that this ejecta could not get into the OPE line of sight if the impact was on the *Giotto* solar arrays. The majority of the fast ejecta leaves the surface at around  $60^\circ$  to the surface normal (Eichhorn 1978) and hence would not be able to enter the OPE line of sight.

The impact explanation offered by Le Duin et al. (1996) requires small ( $\sim 1\text{-}\mu\text{m}$ ) particles to supply enough total cross-sectional area without the total mass ejected becoming unreasonable. However, ongoing studies of  $\sim 5 \text{ km s}^{-1}$  light gas gun impacts using comparable-sized impactors on glass targets at the University of Kent (e.g. Taylor & McDonnell 1997) show that the spallation products tend to be much bigger than the  $\mu\text{m}$ -sized regime needed for the OPE impact scenario, with mm-size fragments being typical. There *would* be  $\mu\text{m}$ -sized ejecta but this would be as part of the fast ejection component travelling at tens of  $\text{km s}^{-1}$ .  $\mu\text{m}$ -sized ejecta travelling at a few tens of  $\text{m s}^{-1}$ , from a  $14 \text{ km s}^{-1}$  impact, do not appear to be physically viable.

The proposed impact site used in the modelling of Le Duin et al. (1996) is positioned exactly on the rear edge of *Giotto*, so allowing (at least potentially) ejecta products to form a spherical shell (hence with some fragments travelling down the OPE line of sight). The solar arrays of *Giotto* did not extend right to the edge of the spacecraft structure (they finished about 2 cm from the edge) and so this geometry precludes the solar array glass fragments getting into the OPE line of sight. The solar panel substructure (i.e. the spacecraft body itself) was made of aluminium honeycomb with glass fibre face sheets. If we allowed the last 1 cm of this structure to undergo impact fragmentation to produce some glass fibre fragmentation products, then one can perhaps envisage some fragments entering the OPE line of sight. However this potential target area constitutes only around 0.5 per cent (max) of the total resolved spacecraft area (as seen by an impacting dust particle). It seems somewhat contrived to have this impact geometry for all the OPE events, and yet not to have detected more particles by DIDSY which presented a much greater detector area. This is in addition to the fragment size and velocity problems mentioned above.

In terms of impact geometry, we think the most likely site for an impact which allows ejecta to travel down the OPE line of sight is the antenna tripod (with the GRE particle impacting the part of the tripod nearest the edge of the solar arrays). The tripod is spinning with the spacecraft, but can present up to  $\sim 6$  per cent of the total spacecraft resolved area (although only about 0.5 per cent at any one time would be consistent with the probable GRE particle impact site of Pätzold et al. 1993). The tripod was made of carbon

reinforced plastic box section structure, and most of the velocity/spallation comments above would apply here also. There is the possibility of the impactor passing straight through the box section producing fragments from the exit hole in the second surface (see e.g. Christiansen 1990) although again geometry precludes the entry of these fragments directly into the OPE line of sight. A similar argument is appropriate to the antenna dish which was made of aluminium honeycomb with carbon reinforced plastic skins. The dish was despun and thus maintained a constant resolved area at encounter of  $\sim 5$  per cent of the spacecraft total.

These considerations lead us to conclude that the impact-generated ejecta cloud model suggested by Le Duin et al. (1996), while superficially appealing, requires more work on the possible impact geometries to specific spacecraft structures, and a mechanism for production of slow-moving  $\mu\text{m}$ -sized ejecta from a  $14 \text{ km s}^{-1}$  impact, before it can be conclusively accepted. We feel it is *one* possible explanation, but alternative explanations also need to be considered. Le Duin et al. quickly dismiss cometary explanations for the OPE events as ‘ad hoc’. They also say that cometary jets would have to have unexpected dust spatial distributions, but do not investigate the effect of various geometries of jets. We will now describe a detailed geometrical dust jet model in order to investigate the possibility of the OPE events being of cometary origin, so offering one alternative explanation for the OPE events.

## 8 COMETARY EXPLANATION FOR EVENTS

### 8.1 Coma–jet model

In order to assess the geometrical possibility of cometary coma features giving rise to the overall shape of the OPE data and also the ‘events’, a model was constructed where asymmetric emission and dust jet activity can be accommodated, and the relative brightness observed by the OPE telescope on board *Giotto* could be simulated. In the model, the background cometary coma of light-scattering grains was assumed to be spherically symmetric (where the spatial density of scattering particles varies as the inverse square of the cometocentric distance). Complex structure (and sunward-biased emission, more akin to that obtained in fountain models) was obtained by superimposing, on this spherical coma, dust jets which can have various widths, directions and emission weightings. By using very wide ‘jets’, global asymmetric emission could be simulated.

Consider a jet, as shown in Fig. 8, initially assumed to be a simple cone pointing in a direction given by spherical polar coordinates  $\phi$ ,  $\theta$ . The jet half-width angle (i.e. half the conic apex angle) is denoted by  $w$ , with the conic jet subtending a total solid angle of  $\Omega$ . Scattering grains are assumed to flow radially and uniformly away from an active region on the nucleus such that the spatial density of scattering grains along the cone falls with an inverse square law. No curvature of the jet due to radiation pressure need be considered as this model concentrates on the near-nucleus region (within 1000 km or so of the nucleus). If one normalizes the total emission of scattering grains from the nucleus to unity, then the fraction of material emitted in the jet is  $f_j$ . The fraction of the total emission accounted for by the remaining material in the general coma is then  $f_c$ , given by  $1 - f_j$ . Hence the relative emission per steradian for the jet and coma respectively is given by  $E_j = f_j/\Omega$  and  $E_c = f_c/4\pi$ . Many jets can thus be incorporated with relative emissions given by  $f_{j1}, f_{j2}, f_{j3} \dots f_{ji}$ , such that

$$f_c + \sum_i f_{ji} = 1. \quad (3)$$

In this model, the scattering properties of the material are assumed to remain constant with time over the period of the encounter. Noting that the phase angle is constant for the viewing geometry from the *Giotto* spacecraft throughout the encounter, the contribution to the observed brightness from a unit volume element of space (which is in the OPE field of view) is simply proportional to the number of grains  $n$  within the element (i.e. spatial number density) and inversely proportional to the square of the distance  $l$  from the spacecraft to the element. Although it is convenient here to express the emission functions and scattering in terms of numbers of particles (implying identical particle properties with emission direction) the model is in fact more general if we consider  $n$  to be proportional to the amount of light scattered (i.e. proportional to the albedo–area product). Therefore, if the particle properties within jets are different from the average coma emission, then the difference in scattering properties is implicit in the value of  $f_j$ .

In order to make the jet model more physical, the simple conic visualization is replaced with a jet such that the angular density profile is Gaussian in nature. This is depicted by the inset graph in Fig. 8. For any given distance  $r$  from the nucleus, the relative spatial density  $n(\psi, r)$  of scattering particles as a function of angular distance  $\psi$  from the jet direction vector is shown for the conic jet and the Gaussian jet. The simple conic jet, of half-width  $w$ , has a square angular profile, whereas the more realistic jet has a Gaussian profile.

The total emission in the Gaussian jet must still be equal to  $f_j$ , and this is satisfied by ensuring that the Gaussian angular profile retains the same peak height, and that the standard deviation of the profile is equal to  $w/\sqrt{2}$ .

The relative brightness contribution of a given unit volume element of space is proportional to the total number  $N$  of grains in the element, where  $N$  consists of  $n_C(r)$  particles from the general coma background, and  $n_{ji}(\psi_i, r)$  particles from the  $i$ th jet present (each jet being angular distance  $\psi_i$  from the volume element being considered) such that

$$N = n_C(r) + \sum_i n_{ji}(\psi_i, r). \quad (4)$$

The contribution to particle number from the general coma is given by

$$n_C(r) = \frac{R_0^2 f_C}{r^2 4\pi}. \quad (5)$$

As we are working in arbitrary units, the constant  $R_0$  (which has units of length) can be put to unity. For the  $i$ th jet, which has emission fraction  $f_{ji}$  and associated width  $w_i$  and hence subtends a solid angle  $\Omega_i$ , the contribution is given by

$$n_{ji}(\psi_i, r) = \frac{R_0^2 f_{ji}}{r^2 \Omega_i} \exp \frac{-\psi_i^2}{w_i^2} \quad (6)$$

with  $R_0$  again put to unity.

The relative intensity contribution  $B$  from material in a given unit volume element, which is in the field of view of the OPE telescope at distance  $l$  from it, is then given by

$$B = \frac{L_0^2 N}{l^2}. \quad (7)$$

As above,  $L_0$  is a constant (with units of length) that can be put to unity.

To obtain a relative OPE lightcurve, points along *Giotto*'s trajectory are selected. At each point, the relative brightness contributions from all volume elements within the OPE telescope field of view are added. The OPE field of view is a narrow cone of

half angle  $\alpha$ , equal to  $1.3^\circ$ , and so for simplicity it is sufficient to consider contributions from 'slices' of the conic field of view as a whole (see Fig. 8) where the spatial density distribution of particles associated with the background coma or jets is assumed to be constant within a given slice of the conic field of view. At any specific point at distance  $l$  along the line-of-sight direction, the point lies within an associated volume element which contributes a relative brightness  $B$ . The total relative intensity contribution  $B_{\text{OPE}}$  is therefore described by

$$B_{\text{OPE}} = \int_0^{l_{\text{max}}} B \pi (l \tan \alpha)^2 dl. \quad (8)$$

As  $B$  is proportional to  $1/l^2$ , then the relative brightness contribution from each slice is independent of distance  $l$ , and just dependent on cometocentric distance  $r$ . The relative intensity contribution  $B_{\text{OPE}}$  is obtained by performing the numerical integration along the OPE line of sight given by (with constants put to unity)

$$B_{\text{OPE}} = \sum_{l=0}^{l_{\text{max}}} \left[ \frac{f_C}{4\pi r^2} + \sum_i \frac{f_{ji}}{\Omega_i r^2} \exp \frac{-\psi_i^2}{w_i^2} \right]. \quad (9)$$

The distance  $l_{\text{max}}$  is the maximum distance along the line of sight for which brightness contributions are added. If the coma were an infinitely extended homogeneous optically thin cloud, then each slice of the conic field of view would give an equal brightness contribution regardless of its distance  $l$  from the telescope. However, as the brightness contribution essentially goes with  $1/r^2$  as shown in equation (9), then for any point along the *Giotto* trajectory within around 1000 km of the closest approach point, and for closest approach distances within a few hundred km, the brightness contribution  $B_{\text{OPE}}$  has fallen to around 1 per cent of the near-field value when  $l \sim 10\,000$  km. (Note that the contribution  $B_{\text{OPE}}$  at  $l=10\,000$  km may in fact be much less if the field of view includes the near-nucleus region.) In the numerical integration,  $l_{\text{max}}$  was therefore put to 10 000 km.

Running the model for the case where there is *only* a spherically symmetric coma yields results that do not fit the observed data well. Fig. 9(a) shows a representation of the spatial density distribution of the modelled spherically symmetric, ' $r^{-2}$ ' coma, for a  $\pm 250$  km 'slice' along the  $x$ - $y$  plane. Although this plot shows the density variation at  $z = 0$  only, whereas the OPE telescope samples space with a range of  $z$  values, it nevertheless offers a useful visualization of the emission function of the comet. The vertical axis represents the spatial density of scattering particles. Fig. 9(b) shows the modelled fit against the OPE data for two test fits using different values of  $x_0$  and  $z_0$ . As one might expect, a simple  $r^{-2}$  coma is inadequate to fit the data.

It is clear that the OPE telescope sampled a significantly more asymmetric near-nucleus coma than a simple spherically symmetric model would suggest. In the jet model described above, broad asymmetries in emission function can be simulated by superimposing one (or more) broad jets on the  $r^{-2}$  background coma. We would expect most of the emission to be towards the sunward hemisphere (i.e. sunward of the  $z$ - $y$  terminator plane) but need not expect perfect symmetry about the sub-solar direction (the  $x$  axis). Fig. 9(c) shows the spatial density representation as in Fig. 9(a), but now a broad jet has been added to the  $r^{-2}$  background coma. This 'jet' has a half-width  $\omega$  of  $40^\circ$ . Broad jets were seen from HMC images at the *Giotto*–Halley encounter, with three major jets having half-widths of  $37^\circ$ ,  $31^\circ$  and  $44^\circ$ , accounting for 0.75 of the observed intensity (Keller et al. 1994). The modelled jet accounts for 0.8 of the total modelled emission, and is in the direction defined by  $\phi = 60^\circ$  and  $\theta = 50^\circ$ . Although these angles are perhaps larger than might be

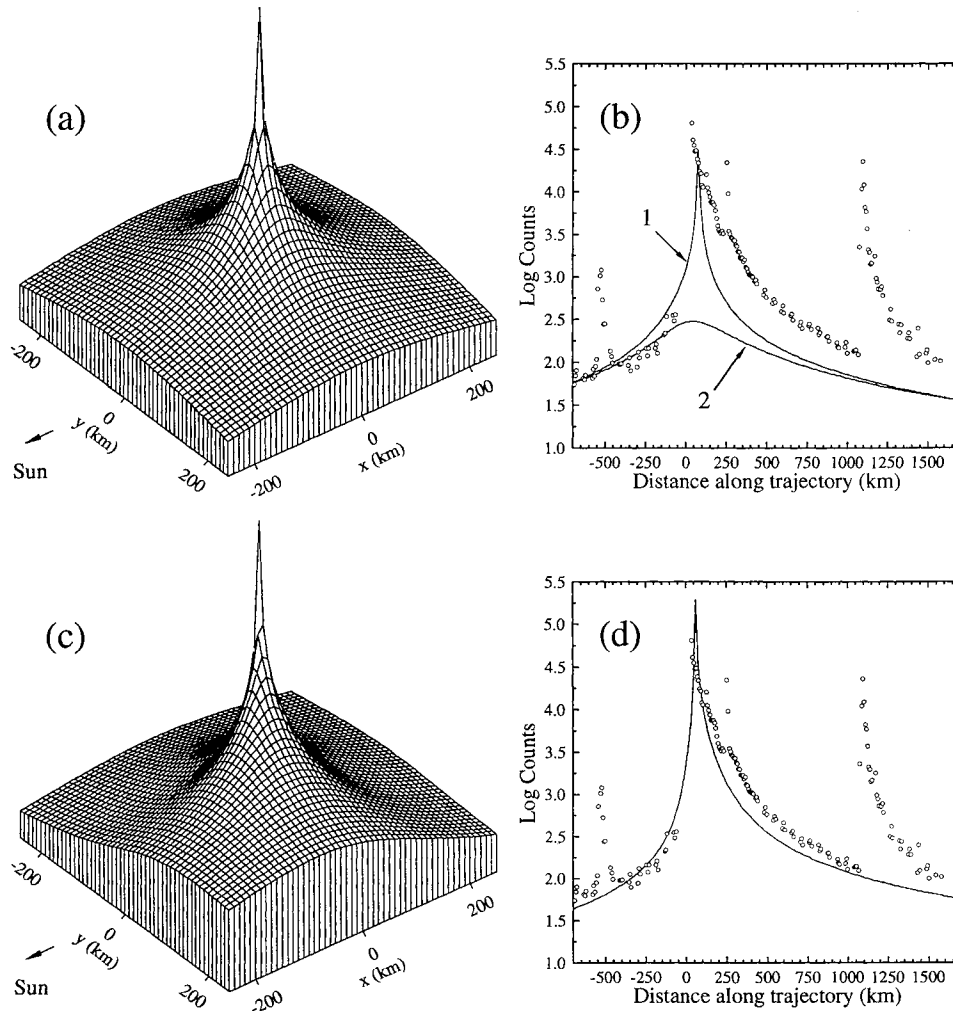


**Figure 9.** The dust spatial density distribution of the  $x$ - $y$  plane containing the nucleus, with the resulting OPE relative intensity. (a) and (b) are fits using a simple  $r^{-2}$  spherically symmetric coma. The curve labelled 1 in (b) corresponds to a geometry of  $x_0 = 0$  km and  $z_0 = 200$  km, whereas the curve labelled 2 corresponds to a geometry of  $x_0 = 200$  km and  $z_0 = 0$  km. (c) and (d) are fits where an asymmetric coma is modelled by superimposing a wide ‘jet’ (characterized by  $\phi = 60^\circ$ ,  $\theta = 50^\circ$ , half-width  $\omega = 40^\circ$ ,  $f_j = 0.8$  and flyby geometry given by  $x_0 = 125$  km and  $z_0 = 75$  km).

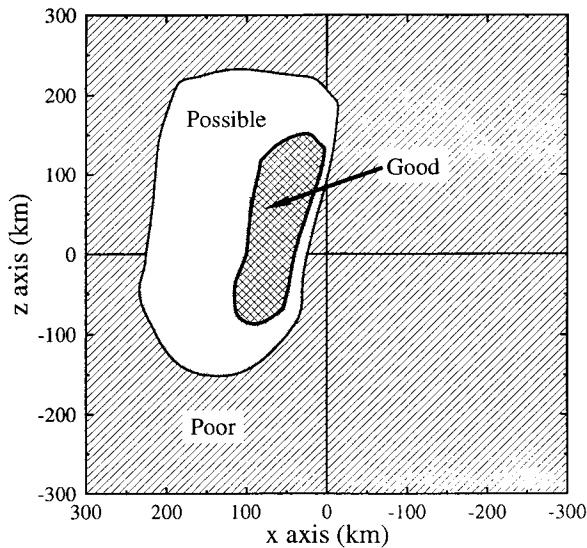
expected, they could be physically viable since they are on the sunward side of the nucleus. Jets are seen on the Halley HMC images at significant angles from the sunward direction, with the maximum emission occurring around  $45^\circ$  from the sunward direction, and significant emission at  $\sim 90^\circ$  (Keller et al. 1994).

Fig. 9(d) shows the modelled result obtained if *Giotto* were to fly through this asymmetric coma, if  $x_0 = 125$  km and  $z_0 = 75$  km. The broadly asymmetric coma gives a much more promising fit to the overall shape of the data. Le Duin et al. (1996) state that a strict  $r^{-1}$  dust coma brightness radial dependence law is found, with their fig. 3 suggesting that even exponents of  $-0.95$  or  $-1.05$  would not give good fits. However, the model fits in their fig. 3 should have been fitted to all of the wings of the OPE data rather than just the peak. We find that an exact exponent of 1.0 is not critical, although our superimposed asymmetric inner coma does not conflict with good fits to the OPE data obtained in the outer coma using  $r^{-1}$ .

By running the model for many values of  $x_0$  and  $z_0$  and for many orientations and emission weightings of a single broad jet, a feel for the likely encounter orientation is developed (i.e. the most likely range of  $x_0$  and  $z_0$  values). A fit is judged ‘good’, ‘possible’ and ‘poor’ by using a least-squares method. Fig. 10 shows the broad regions in the  $x$ - $z$  plane through which *Giotto* would have passed,

with the most likely areas highlighted. The ‘good fit’ region is the most likely region where *Giotto* passed, although the ‘possible’ region cannot be ruled out (but it is unlikely). From the modelling, it is highly unlikely that *Giotto* could have passed through the ‘poor fit’ region, and this is effectively discounted. Also, for the ‘good fit’ region, the areas with a positive  $z$  value are somewhat more favourable. From this modelling, it is virtually certain that *Giotto* passed on the sunward side of the terminator plane at closest approach (i.e. that *Giotto* crossed the terminator plane after closest approach) and it is likely that *Giotto* passed in the positive  $z$  region such that the sunward, near-nucleus region would be within the OPE field of view. The best fits are obtained with closest approach distances of around 100 km, although distances up to 300 km cannot be discounted.

A more conceptually realistic model of the near-nucleus dust coma is obtained by allowing two broad jets to be superimposed upon the  $r^{-2}$  background coma. Fig. 11(a) shows the relative dust spatial density in the  $x$ - $y$  plane (as before) produced by incorporating two broad ‘coma-jets’; one directly towards the sunward direction and a broader, weaker jet  $\sim 40^\circ$  from the sunward direction. Parameters of these two jets are given in the ‘coma-jet’ columns of Table 6.



**Figure 10.** Quality of fit for solutions corresponding to various  $x_0$  and  $z_0$  encounter geometries. The fits are performed with one wide jet superimposed upon a symmetric  $r^{-2}$  coma (as in Fig. 9c) with various jet modelling parameters.

*Giotto* can be envisaged passing through this modelled coma, and the modelled OPE brightness curve that would result is shown in Fig. 11(b). The result shown is for *Giotto* passing through the  $x$ – $z$  plane at  $x_0 = 125$  km and  $z_0 = 75$  km (closest approach distance about 140 km). It should be noted that the fit shown in Fig. 11(b) is not unique, and similarly good fits are obtained with different values of  $x_0$  and  $z_0$  with slightly different coma–jet parameters, within the range described above by the ‘good’ or ‘possible’ fits.

We have seen that the overall shape of the data set can be fitted reasonably well, indicating an asymmetric coma in the near-nucleus region. We now investigate the plausibility of explaining events 1, 2 and 3 by the presence of thin dust jets or ‘filaments’. Upon the fit shown in Fig. 11(a), we can introduce three additional jets. Table 6 gives the jet parameters, marked as event 1, 2 and 3. Fig. 11(c) shows a plan view of the orientation of the jets (i.e. as seen if viewing from the positive  $z$  axis direction). The figure shows the two broad coma–jets, and the three thin additional jets needed to model the data, with *Giotto*’s trajectory overlaid. The OPE line of sight is within  $22^\circ$  of being directly into the paper. Fig. 11(d) shows the resulting fit using the additional jets. All three events require very narrow jets with the jet half-width being around  $1^\circ$ . This scenario is perhaps physically viable considering the jet filaments that are observed on enhanced HMC images (Keller et al. 1994), these

structures having a width of  $\leq 3^\circ$ . Events 1 and 2 have pointing directions from the sunward direction of about  $67^\circ$  and  $72^\circ$  respectively. However, event 3 has a pointing direction of about  $94^\circ$  from the sunward direction, i.e. the jet is actually anti-sunward of the terminator plane. The jet is also extremely thin with conic half-width around  $0.1^\circ$ . It is hard to imagine that these modelled parameters for event 3 are characteristics that would be found in reality. It is also apparent from Fig. 11(d) that the event 3 jet does not fit the profile shown in the OPE data. Indeed, we could not fit the profile at all with a simple jet as used in the model, and we do not feel that a jet with an angular density profile which departs from a Gaussian form by an extraordinary amount is physically viable. Another problem is the sheer strength of the feature. It is difficult to envisage a physical jet that could give a contribution of such intensity when, even with the most accommodating encounter geometry, the line of sight and hence the material being viewed in the jet could be no less than  $\sim 1000$  km from the nucleus.

## 8.2 Possible nucleus fragments

It has been suggested (Lvasseur-Regourd et al. 1993b; McBride & Lvasseur-Regourd 1994) that event 3 may have been caused by *Giotto* passing close to a secondary source of cometary brightness i.e. a significant cometary fragment. If this is the case, the position of the fragment is no longer so constrained by the encounter geometry, in that *Giotto* could pass very near to it even though it is  $\sim 1100$  km after the closest approach to the parent nucleus. To investigate whether this scenario is consistent with the observed profile of the feature, the model was adapted so a cometary fragment could be incorporated.

Envisage a fragment lying at coordinates  $x_f, y_f, z_f$  in the frame as depicted in Fig. 1. This fragment has a total emission of scattering grains equal to a fraction  $F$  of the emission of the parent nucleus. The fragment can then be considered in the same way as the parent nucleus, with an associated spherically symmetric background coma, and a number of jets emanating from the surface. Using the same nomenclature as before, but denoting terms resulting from the fragment with a prime superscript, the relative emissions of jets from the fragments can be written  $f'_{j1}, f'_{j2}, f'_{j3} \dots f'_{ji}$ , such that

$$f'_C + \sum_i f'_{ji} = 1, \quad (10)$$

where  $f'_C$  is the relative fraction of emission accounted for by the background coma, as before. For a given point along *Giotto*’s trajectory, the integration along the line of sight can be performed as before, but incorporating the fragment’s contribution (treated as a relatively weak secondary nucleus with  $k$  jets) such that equation (9)

**Table 6.** The parameters of the jets used in the model fits. For these fits, the *Giotto*–nucleus geometry is defined by  $x_0 = 125$  km and  $z_0 = 75$  km ( $a_0 \sim 140$  km). The fragment used to produce Fig. 11(e) is assumed to be 4 per cent (maximum) of the activity of the parent nucleus, and is at  $x_f = -110$  km,  $y_f = 1070$  km and  $z_f = 0$  km. The fragment used to produce Fig. 11(g) is assumed to be  $\sim 1$  per cent of the activity of the parent nucleus, and is at  $x_f = -85$  km,  $y_f = 1050$  km and  $z_f = 25$  km.

Jet parameter	Coma–jet 1	Coma–jet 2	Jet for event 1	Jet for event 2	Jet for event 3	Fragment jet (11e)	Fragment jet (11g)
$\phi$	0.0	33.0	−67.4	72.5	94.3	33	85
$\theta$	90.0	113.0	90.0	90.0	90.0	113	83
$w$	14.0	29.5	0.3	1.0	0.1	35	10
$f_j$	0.721	0.215	0.001	0.025	0.002	0.90	0.95

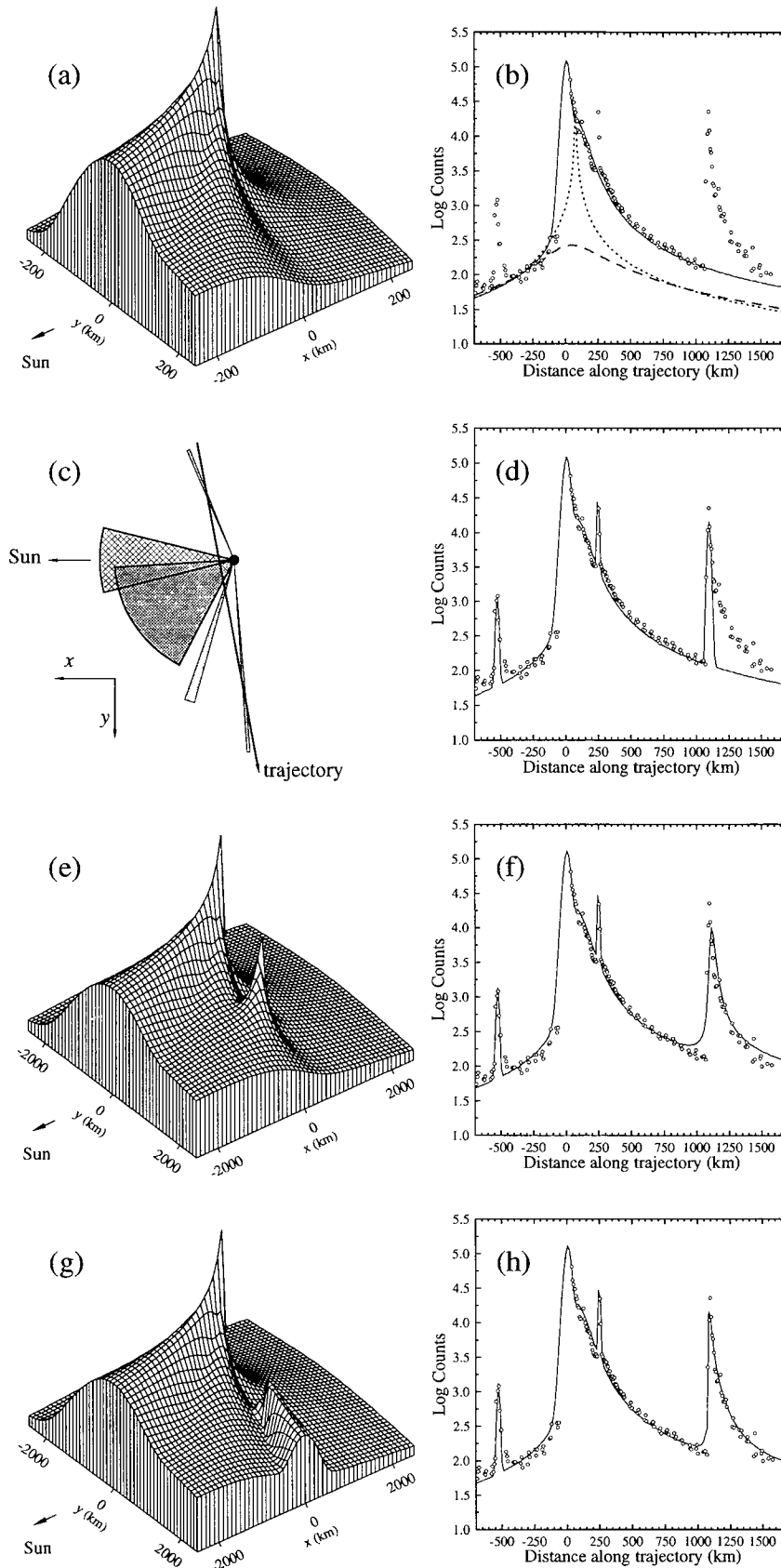


**Figure 11.** The dust spatial density distribution of the  $x$ - $y$  plane containing the nucleus, with the resulting OPE relative intensity. (a) and (b) are fits using two wide jets superimposed upon a  $r^{-2}$  spherically symmetric coma (parameters given in Table 6). The dotted and dashed curves in (b) correspond to the geometries which were labelled 1 and 2 in Fig. 9(b). (c) and (d) show fits where three additional thin jets are added to the fit. (e) and (f) show the fit when event 3 is then modelled by a nucleus fragment, giving rise to its own local asymmetric coma. (g) and (h) show the fit when the fragment has mostly asymmetric emission. See text for details.

becomes

$$B_{\text{OPE}} = \sum_{i=0}^{i_{\text{max}}} \left[ \frac{f_C}{4\pi r^2} + \left( \sum_i \frac{f_{ji}}{\Omega_i r^2} \exp \frac{-\psi_i^2}{w_i^2} \right) + \frac{Ff'_C}{4\pi r^2} + \left( \sum_k \frac{Ff'_{jk}}{\Omega_k r^2} \exp \frac{-\psi_k^2}{w_k^2} \right) \right], \quad (11)$$

where  $r'$  is the distance from the fragment to the field of view slice being considered,  $\Omega'_k$  is the solid angle subtended by the  $k$ th fragmentary jet, and  $w'$  is the associated half-width of that jet.

As the feature is observed  $\sim 1100$  km after closest approach, then the position coordinates of the fragment are likely to be such that  $y_f$  is also around 1100 km, and  $x_f$  is negative. Hence the OPE field of view will pass close to the fragment. It is reasonable to assume that a fragment may also have asymmetric emission. In leaving the parent nucleus, relatively large areas of previously unexposed material will be presented to the solar flux. One can even envisage the possibility of one side of the fragment being active, and the other side essentially inactive. This, partnered with the possibility that the fragment could be spinning at a relatively high rate, suggests that emission could indeed be very asymmetric.

Fig. 11(e) shows the representation of the spatial density distribution of the modelled coma as was shown in Fig. 11(a), but the base plane scale has now been extended out to  $\pm 2500$  km, and a fragment is present. The fragment is modelled such that it has its own  $r^{-2}$  coma, plus a broad jet which is within  $45^\circ$  of the Sun direction (the total emission is around 4 per cent that of the parent comet). The parameters of this jet with respect to the fragment are given in Table 6 in the second to last column. Fig. 11(f) shows the resulting fit to the data.

Fig. 11(g) shows a fragment but with a somewhat narrower jet which is pointing about  $85^\circ$  from the Sun, giving a more asymmetric emission. In this case the total fragment emission is  $\sim 1$  per cent that of the parent comet. We are not necessarily suggesting that this modelled jet represents a realistic physical scenario, but present the fit to demonstrate that the profile of event 3 can conceivably be fitted well. In reality, the fragment–jet structure might be more complex than one simple radial jet can represent. Indeed, with a spinning fragment one may expect a very complicated fragment–coma structure, with perhaps curved jets due to the ‘garden sprinkler’ effect (not radiation pressure).

We conclude that the inclusion of a cometary fragment can offer a possible explanation for the event 3 profile seen in the OPE data. The modelled fragment emission is of order 1 per cent that of the main nucleus, although it is important to note that this value corresponds to the fraction of the *modelled* nucleus emission and thus probably represents an upper limit (i.e. the OPE line of sight almost certainly did not sample all the jets present and so some of the *real* Grigg–Skjellerup emission will not have been included in the model). The fit presented in Fig. 11(f) is for a geometry such that *Giotto* passed about 50 km from the fragment. If however *Giotto* passed much closer (say just a few km), then intuitively one would expect the emission figure to be much lower. However, the OPE line of sight is conical (as in Fig. 8) and so if the instrument passes close to an extended source, although the near-field source may be bright, the instrument sees less of it. Hence, in the model, even if the *Giotto*–fragment miss distance is very small, one still needs of order 1 per cent of the nucleus emission to get a realistic fit to the event 3 profile. For these reasons, the value of order 1 per cent emission of the nucleus is reasonably geometry-independent. A crude estimate of the size of the fragment can therefore be made. If

we assume a nucleus of diameter of 1 km with 1 per cent of its surface active, with the fragment having perhaps 50 per cent of its area active, then (assuming the active areas have similar emission characteristics) the radius of the fragment would be  $\sim 10$  m. If however we assume a larger radius, say 2 km diameter, and with 10 per cent of its area active, then the fragment would have a radius of  $\sim 100$  m.

## 9 DISCUSSION

The significant asymmetry and structure in the OPE data need to be explained. We have seen that the profile of event 1 is inconsistent with ejecta from a cometary particle impact on *Giotto*. The closest-approach region is clearly complex with exact determination of the causative mechanism difficult. However, it does appear possible that the striking profile of event 3 could be consistent with a cometary dust impact scenario as investigated by Le Duin et al. (1986), and the timing of the main OPE brightness does appear correlated with the GRE particle impact (although almost by definition this will also coincide with the maximum cometary dust density and structure). This explanation is appealing, although considerations of the hypervelocity impact mechanisms and impact geometry show that this explanation is not without problems, and some more work is needed before it can be conclusively accepted.

As an alternative solution, the modelling presented here indicates that the innermost coma of Grigg–Skjellerup may have been complex with significant structure and jet activity. It must be stressed that the modelled results presented are not unique, and the suggested presence of cometary jets is not in itself contrived (after all, similar modelling of the complex near-nucleus jet region of Comet Halley would appear contrived were it not for the existence of the HMC images). The data also indicate possibly the first *in situ* detection of a significant cometary fragment. These two results are perhaps self-consistent in that if a fragment (or perhaps *fragments*) had detached itself from the parent nucleus, one may expect the nucleus to have relatively large areas of newly exposed cometary material. It is also possible that the presence of fragments may indicate a relatively short spin period. These considerations would be wholly consistent with the observed high degree of asymmetry in the innermost coma, and also with the modelled result that significant emission may hence occur in directions at quite large angular distances from the subsolar point.

The fragment scenario is also supported by the polarization data (Fig. 3), which suggests different explanations for the different events. The increase in polarization for events 1 and 2 is consistent with changes in the size distribution as a result of jet activity (Eaton, Scarrott & Warren-Smith 1988). However, event 3 is more analogous to the decrease in polarization seen close to a ‘nucleus’, and observed for the main peak in the OPE data.

Grigg–Skjellerup was observed during the 19th century. Since then it has been identified with comet 1808III Pons (Kresak 1986). Pons had suspected an unusual ‘very faint nucleus in two parts’ (Pons 1829) and, more significantly, irregularities in the comet’s lightcurve and low relative mass loss suggest an advanced crusting of the surface of the nucleus (Kresak 1987). Other observations are described by Hughes (1991).

At its 1992 return, the comet was observed by Jockers et al. (1993) about eight hours after closest approach, and by Fulle et al. (1993) a few days after the flyby. The anisotropy of the dust coma was also noticed. The power-law exponent of the radial dependence of the dust brightness, found to be about  $-1.25$  tailward and  $-1.7$  sunward, has been computed to correspond to  $-0.95 \pm 0.2$  and

$-1.7 \pm 0.2$  for the *Giotto* observations, in good agreement with the OPE results (Fulle et al. 1994).

Since the comet–Earth distance was 1.4 au and since the elevation was low above the horizon, the resolution was not better than 1600 km (1.5 arcsec) at the coma for the ground-based observations. Any fragment, at about 1100 km from the nucleus, observed against the high surface brightness background due to the coma would therefore be impossible to detect directly. Emission from the exposed ices on the fragment would be indistinguishable from emission from the nucleus itself, and would perhaps be interpreted as jet activity or an outburst. Our *in situ* results are therefore not inconsistent with the ground-based observations. The possible detection of cometary fragments needs however to be assessed from observations of other comets.

Though perceived as rare by observers, fragmentation and splitting seems to be a common occurrence in comets (Chen & Jewitt 1994). The most famous recent case of splitting is that of Shoemaker–Levy 9, which had been captured by Jupiter some decades ago, and was tidally disrupted when it passed at less than 40 000 km from the upper atmospheric layer of the giant planet in 1992 July. Although some fragments were found to suffer secondary splitting, it is not yet possible to choose between models describing the parent nucleus as a strengthless agglomerate of subnuclei only held by gravity, or as a discrete body with low tensile strength in which fissures easily propagated (Donn & Hughes 1986; Scotti & Melosh 1993; Solem 1994; Sekanina 1995). Observations using the *Hubble Space Telescope* (*HST*) suggest that several sizeable companions might have been detected within 1000 km of the projected location of the brightest fragment (Sekanina 1995), and that at least four fragments in the 0.3- to 0.7-km size range impacted Jupiter in 1994 July (Weaver et al. 1994).

Comet Brooks 2 has also been found to break apart due to the action of tidal forces of Jupiter and members of the Kreutz family (sungrazing comets) have suffered fragmentation because of the action of the Sun (Marsden 1989). However, tidal forces do not appear to be a common disruption mechanism for about 30 well-documented comet splits. It has been suggested that some fragments contain a very minor fraction of the main nucleus, typically 1 per cent or less, and that some ‘peel off’, or that ‘crust-loss’ mechanisms take place (Sekanina 1982; Hughes & McBride 1992).

When cometary fragments are significant compared to the parent nucleus, the fragmentary event will be interpreted as ‘comet splitting’. The recessional velocity of a significant nucleus fragment from its parent nucleus will be relatively low compared with the ejection speeds of meteoroids in the sub-cm size regime (which are relatively well coupled with the cometary gas outflow). Sekanina (1982) considered 21 known comet splitting events and for the few events where the magnitude of the recessional velocity could be deduced, a mean of order  $1 \text{ m s}^{-1}$  is determined. With an ejection velocity of  $1 \text{ m s}^{-1}$ , a fragment observed at a distance of 1100 km from the nucleus might have been ejected about 13 d before. The lifetime of a fragment, which depends upon its diameter  $D$ , heliocentric distance and orbital characteristics, has been estimated to be of the order of  $0.6D/10 \text{ yr}$  at 1 au, with  $D$  in m (Chen & Jewitt 1994). An object of order 10 m would easily survive the loss of volatiles by sublimation during less than one month.

Recent observations of Comet C/1996B2 Hyakutake have indicated some very interesting features with respect to possible nucleus fragmentation. Lecacheux et al. (1996) reported luminous knots slowly receding from the nucleus region on 1996 March 24; these ‘objects’ having a cometocentric velocity of  $12 \text{ m s}^{-1}$ . The

knots persisted to around 2340 km from the nucleus region. Tozzi et al. (1996) report observing ‘a blob’ on 1996 March 25 at 1350 km from the nucleus region, receding at  $17 \text{ m s}^{-1}$ . Feldman et al. (1996) derive from *International Ultraviolet Explorer* (*IUE*) observations that the nucleus had lost some fragments. Sekanina (1996) has suggested that a fragment separated from the nucleus on 1996 March 21. Harris et al. (1996) report the nucleus region separating into two distinct features (observed 1996 March 26), although it should be noted that *HST* images taken around 1996 March 26 do not support this (Weaver et al. 1996) but do appear to show remnants of the ‘knots’ seen by Lecacheux et al. (1996) two days earlier.

Although a comparison of a comet like C/1996B2 Hyakutake with P26/Grigg–Skjellerup needs to be treated with caution, it does however underline the friability and fragility of comets, and that the behaviour of fragments leaving the surface of the nucleus is likely to be quite common. We suggest that the nucleus fragment explanation of the OPE features is not as unlikely as it may first appear, and that this should certainly be considered in the mission strategies of the *Rosetta* and *Stardust* cometary probes.

## ACKNOWLEDGMENTS

We thank Emma Taylor (University of Kent) for discussions on brittle material impacts, Mark Herbert (Matra Marconi Space UK) for *Giotto* structure information, and David Hughes for helpful comments to improve this manuscript. NM would like to thank the UK Particle Physics and Astronomy Research Council (PPARC) for financial support. Some of the modelling was performed using the Starlink network (Starlink is funded by PPARC). ACLR would like to thank the dedicated efforts of the European Space Agency teams during the Grigg–Skjellerup encounter, and the support provided by the French Programme National de Planetologie.

## REFERENCES

- Asay J. R., Shahinpoor M., eds, 1993, High-pressure shock compression of solids. Springer-Verlag, Berlin
- Chen J., Jewitt D., 1994, *Icarus*, 108, 265
- Christiansen E. L., 1990, *Int. J. Impact Eng.*, 10, 125
- Divine N., 1981, ESA SP-174, p. 25
- Divine N., 1983, JPL, IOM (Interoffice Memorandum) 5137-83-294
- Divine N., 1985, JPL, IOM (Interoffice Memorandum) 5137-85-234
- Donn B., Hughes D. W., 1986, ESA SP-250, p. 523
- Eaton N., Scarrott S. M., Warren-Smith R. F., 1988, *Icarus*, 76, 270
- Eichhorn G., 1978, *Planet. Space Sci.*, 26, 469
- Feldman P. D., Festou M., Rodriguez P. M., Gonzalez R., 1996, *IAU Circ.* 6370
- Fulle M., Menella V., Rotundi A., Colangeli L., Bussoletti E., Pasian F., 1993, *A&A*, 276, 582
- Fulle M., Menella V., Rotundi A., Colangeli L., Bussoletti E., 1994, *A&A*, 289, 604
- Giovane F. et al., 1991, *Appl. Optics*, 30, 2579
- Goidet-Devel B., 1994, PhD thesis, Université de Paris 6, France
- Goidet-Devel B., Clairemidi J., Rousselot P., Moreels G., 1997, *Icarus* 126, 78
- Harris W. M., Schlerb F., Percival J. W., Nordsieck K., Mueller B. E. A., Harmer D., MacDonald A., 1996, *IAU Circ.* 6360
- Hughes D. W., 1991, *Vistas Astron.*, 34, 1
- Hughes D. W., McBride N., 1992, *J. Br. Astron. Assoc.*, 102, 265
- Jockers K., Kiselev N. N., Boehnhardt H., Thomas N., 1993, *A&A*, 268, L9
- Kadono T., Fujiwara A., 1986, *J. Geophys. Res.*, 101, 26097
- Keller H. U., Curdt W., Kramm J.-R., Thomas N., 1994, in Reinhard R., Longdon N., Battrick B., eds, *Images of the Nucleus of Comet Halley*. ESA SP-1127, p. 82

- Kresak L., 1986, IAU Circ. 4234  
 Kresak L., 1987, Bull. Astron. Inst. Czech., 38, 65  
 Kruger F. R., 1984, ESA SP-224, p. 49  
 Lecacheux J., Jorda L., Enzian A., Klinger J., Colas F., Frappa E., Laques P., 1996, IAU Circ. 6354  
 Le Duin T., Crifo J. F., Le Quéau D., Crifo F., 1996, A&A, 308, 261  
 Levasseur-Regourd A. C., 1992, in Gérard J. C., Surdej J., eds, Observations and physical properties of small solar system bodies. Institut d'Astrophysique, Liège, p. 141  
 Levasseur-Regourd A. C., Dumont R., 1980, A&A, 84, 277  
 Levasseur-Regourd A. C., Schuerman D. W., Zerull R. H., Giese R. H., 1981, Adv. Space Res., 1, 113  
 Levasseur-Regourd A. C., Bertaux J. L., Dumont R., Festou M., Giese R., Giovane F., Lamy P., Weinberg J. L., 1984, Adv. Space Res., 4, 287  
 Levasseur-Regourd A. C. et al., 1986a, ESA SP-1077, p. 187  
 Levasseur-Regourd A. C. et al., 1986b, Nat, 321, 341  
 Levasseur-Regourd A. C., Goidet B., Le Duin T., Malique C., Renard J. B., Bertaux J. L., 1993a, Planet. Space Sci., 41, 167  
 Levasseur-Regourd A. C. and the OPE team, 1993b, Ann. Geophys., 11, III, C469  
 Levasseur-Regourd A. C., Hadamcik E., Renard J. B., 1996, A&A, 313, 327  
 Marsden B. G., 1989, AJ, 98, 2306  
 McBride N., Levasseur-Regourd A. C., 1994, Ann. Geophys., 12, III, C671  
 McDonnell J. A. M. et al., 1993, Nat, 362, 732  
 Morley T. A., 1991, ESA SP-326, p. 487  
 Pankiewicz G. S., 1989, PhD thesis, Univ. of Kent, Canterbury  
 Pankiewicz G. S. et al., 1989, Adv. Space Res., 9, 273  
 Pätzold M., Edenhofer P., Bird M. K., Volland H., 1993, A&A, 268 L13  
 Pons J. L., 1829, Astron. Nachr., 7 (No. 149), 113–114  
 Renard J.-B., Levasseur-Regourd A.-C., Dollfus A., 1992, Ann. Geophys., 10, 288  
 Renard J.-B., Hadamcik E., Levasseur-Regourd A.-C., 1996, A&A, 316, 263  
 Roach F. E., Gordon J. L., 1973, Geophys. Astrophys. Monogr., 4, 23  
 Schneider E., Stülp A. J., Kagerbauer G., 1995, Int. J. Impact Eng., 17, 731  
 Scotti J. V., Melosh H. J., 1993, Nat, 365, 733  
 Sekanina Z., 1982, in Wilkening L. L., ed., Comets. Univ. Arizona Press, Tucson, p. 251  
 Sekanina Z., 1995, A&A, 304, 296  
 Sekanina Z., 1996, IAU Circ. 6360  
 Solem J. C., 1994, Nat, 370, 349  
 Taylor E. A., McDonnell J. A. M., 1997, Adv. Space Res., in press  
 Toller G. N., 1990, in Bowyer S., Leinert C., eds, The Galactic and extragalactic background radiation. Kluwer, Dordrecht, p. 21  
 Tozzi G.-P., Lisi F., Oliva E., Patriarchi P., 1996, IAU Circ. 6357  
 Weaver H. A. et al., 1994, Sci, 267, 1282  
 Weaver H. A. and *HST* team, 1996, IAU Circ. 6363

This paper has been typeset from a  $\text{T}_{\text{E}}\text{X}/\text{L}^{\text{A}}\text{T}_{\text{E}}\text{X}$  file prepared by the author.